Observations

of the

CALIFORNIA INSTITUTE OF TECHNOLOGY

RADIO OBSERVATORY

Owens Valley, California

1961

4. BRIGHTNESS DISTRIBUTION IN DISCRETE RADIO SOURCES I. OBSERVATIONS WITH AN EAST-WEST INTERFEROMETER

by

Alan T. Moffet

BRIGHTNESS DISTRIBUTION IN DISCRETE RADIO SOURCES I. OBSERVATIONS WITH AN EAST-WEST INTERFEROMETER

by

Alan T. Moffet

California Institute of Technology
Radio Observatory

Owens Valley, California

ABSTRACT

The Caltech variable baseline interferometer has been used in a program of brightness distribution measurements on 195 discrete radio sources at a wavelength of 31.3 cm. This paper reports measurements, made with an east-west interferometer baseline, of the complex visibility functions of 127 sources. The amplitude and phase of the visibility functions were measured at transit with antenna spacings of 195λ, 389λ, 779λ and 1557λ. Using these same basic spacings, and by observing at large hour angles, the visibility amplitude was measured at ten other effective spacings between 126λ and 1363λ. Not all sources were observed at all spacings. The data are presented in tabular form, and graphs of the visibility amplitude as a function of antenna spacing are given for 51 of the more interesting sources. The interpretation of these data in terms of source brightness distributions will be given in another paper.

I. INTRODUCTION

Although several thousand discrete radio sources are listed in current catalogues, detailed brightness distributions are known for only a few. Until recently, pencil-beam antennas have had sufficient resolution to study in detail only the very largest sources, while variable-spacing interferometers with small individual elements have been limited both by low sensitivity and by confusion to studies of only the very strongest sources. Survey interferometers with only two or three fixed spacings have given information about the angular diameters of many sources, but have not provided sufficient information to determine brightness distributions in any detail.

The Caltech variable-baseline interferometer has sufficient sensitivity and primary resolution at a wavelength of 31.3 cm to observe several hundred sources. It has been employed, at this wavelength, in a program of brightness distribution measurements on 195 of these objects. In this paper are reported measurements of source visibility functions made with an east-west interferometer baseline, while the following paper (Maltby 1962) contains the results of similar measurements made with a north-south baseline. Based on these measurements of the source visibility functions, a third paper (Maltby and Moffet 1962) contains interpretations of the brightness distributions in 174 extragalactic and 21 galactic radio sources. A fourth paper (Maltby, Matthews, and Moffet 1962) is concerned with the implications of the observed brightness distributions in a number of sources which have been identified with optical objects.

In the following section of this first paper, various mathematical relationships are set forth which are necessary for an understanding of how a variable baseline interferometer may be used to measure brightness distributions. Some of these relationships are also needed to define the observational data presented in this paper and the next.

II. INTERFEROMETRY OF DISCRETE SOURCES

Methods of studying discrete sources of radiation by interferometry were first set forth by Michelson (1890, 1891), who applied these methods, many years later, in the measurement of stellar diameters (Michelson 1920; Michelson and Pease 1921). Bracewell (1958) has reviewed the radio interferometry of discrete sources, and this discussion will follow his general line of development. It will, however, deal specifically with brightness distribution measurements as they can be made with instruments such as the Caltech interferometer.

a) Geometry of the Interferometer

The Caltech interferometer consists of two equatorially mounted parabolic antennas, each 90 ft in diameter. The mounts may be moved along railroad tracks to certain fixed observing stations. We define the baseline as the line joining the vertices of the two paraboloids. Its length is s wavelengths at the operating frequency, and its azimuth is α. We assume that the baseline is level when both antennas are pointed in the same direction.

The monochromatic response pattern of the phase-switched (Ryle 1952) or a continuous-multiplication interferometer (Read 1961) consisting of two antennas with isotropic sensitivities is a function only of the angle θ between the source direction and the median plane of the interferometer and is

$$R(\theta) = G A \cos(2\pi s \sin\theta + \Psi) , \qquad (1)$$

where A is the collecting area of each antenna, Ψ is an instrumental phase error which must be determined, and G allows for receiver gain changes. The response of a practical interferometer is obtained by averaging this monochromatic response over the receiver passband (Read 1961); in the discussion which follows we will neglect the effects of receiver bandwidth. If the individual antennas do not have isotropic responses, then A must be re-

placed by the product of their voltage responses. If the two antennas are identical, this product is equal to the power response $A(\theta, \psi)$ of one antenna. The angles θ and ψ form a system of spherical polar coordinates having the interferometer baseline as polar axis.

It can be seen that the interferometer response pattern is a series of sinusoidal fringes having a period of $1/s$ in $\sin\theta$, or an approximate period of $1/(s \cos\theta)$ in θ. The product $s \cos\theta$ may be called the effective baseline since it determines the angular fringe spacing is any region of the sky small enough that, within the region, $\cos\theta$ has nearly a constant value.

For astronomical purposes, the response pattern is more conveniently dealt with in terms of hour angle and declination. As is shown in the Appendix, if ϕ is the geographic latitude and α is the aximuth of the baseline, $\sin\theta$ is given by

$$\sin\theta = -\sin\alpha \cos\delta \sin h + \cos\alpha (\cos\phi \sin\delta - \sin\phi \cos\delta \cos h) \quad (2)$$

In two important special cases this expression may be simplified. These are the cases of an east-west baseline, for which $\alpha = \pi/2$ and

$$[E\text{-}W] \qquad \sin\theta = -\sin h \cos\delta \ , \quad (3)$$

and the case of a north-south baseline, for which $= 0$ and

$$[N\text{-}S] \qquad \sin\theta = \sin\delta \cos\phi - \cos\delta \sin\phi \cos h \ . \quad (4)$$

In order to interpret interferometric observations it is necessary to know the orientation of the interference fringes with respect to the source being studied, i.e. with respect to the grid of celestial coordinates in the neighborhood of the source. The fringes lie along curves of constant $\sin\theta$ and hence are normal to the gradient of $\sin\theta$. This gradient is parallel to the local projection of the baseline onto the unit sphere (or the sky), and we will specify the fringe orientation by the position angle[1] p of $\nabla \sin\theta$ at the point in question.

The angle p is given by the relation

$$\tan p = -\frac{(\nabla \sin\theta)_h}{(\nabla \sin\theta)_\delta} = -\frac{(\cos\delta)^{-1} \partial \sin\theta / \partial h}{\partial \sin\theta / \partial \delta} \ ,$$

or

$$\tan p = \frac{-\sin\phi \sin h}{\cos\phi \cos\delta + \sin\phi \sin\delta \cos h} \ . \quad (5)$$

[1] As is customary, the position angle is measured from north, positive through east.

For the two special cases mentioned above, this expression may be simplified. With an east-west baseline, cot p is a more convenient quantity:

$$\left[\text{E-W}\right] \qquad \cot p = \sin \delta \tan h \quad . \tag{6}$$

With a north-south baseline, equation (5) becomes

$$\left[\text{N-S}\right] \qquad \tan p = \frac{-\sin \phi \sin h}{\cos \phi \cos \delta + \sin \phi \sin \delta \cos h} \quad . \tag{7}$$

b) Brightness Distribution and the Visibility Function

Now that the necessary geometric relationships have been established, we can show how the brightness distribution of a radio source may be investigated with a two-element interferometer. A source is located by α_o and δ_o, the coordinates of the centroid of its emission at a specified epoch and wavelength, and it is described in detail by the brightness temperature distribution $T(\alpha-\alpha_o,\delta-\delta_o)$ of that emission. In the neighborhood of a small source, the celestial coordinates will closely approximate a Cartesian grid, and it will simplify the analysis to make this approximation.

Let x,y be a Cartesian coordinate frame fixed in a small region of the sky centered at α_o,δ_o such that x increases toward the east along a circle of declination and y increases toward the north along an hour circle. The units of x and y are radians, and the transformation (approximately valid for $|x|, |y| << 1$) is

$$\begin{aligned} x &= (\alpha - \alpha_o) \cos \delta_o \\ y &= \delta - \delta_o \end{aligned} \tag{8}$$

Using the relation $\alpha = \Omega t - h$, where Ω is the sidereal rate and t the sidereal time, x can be expressed in terms of t and h.

In a similar fashion, the interferometer coordinates θ and Ψ, in the neighborhood of the source, will also approximate a Cartesian system, rotated with respect to the x,y system by the angle $p-\pi/2$, as is shown in Figure 1. In the x,y system, the reponse pattern of equation (1) then becomes

$$R(x,y,t) = G\, A(x,y) \cos \left\{ 2\pi \left[s_x(x - \Omega t) + s_y y \right] + \Psi \right\} , \tag{9}$$

where s_x and s_y are the projections of the baseline onto the x and y axes, i.e. the x and y components of the effective baseline,

$$\begin{aligned} s_x &= s \cos \theta \sin p \\ s_y &= \cos \theta \cos p \quad . \end{aligned} \tag{10}$$

We now wish to decribe the response of the interferometer to a discrete

source passing through its sensitivity pattern. Let the source be described by its brightness temperature distribution[2] $T(x,y)$. This is generally a function of the wavelength of observation λ . The integral of $T(x,y)$ over the source gives the flux density of the radiation from the source at that wavelength.

$$S = 2k/\lambda^2 \iint T(x,y)\, dx\, dy \quad .$$

The response of the interferometer to the source will be given by integrating equation (9) over the source distribution,

$$R(t) = 2k/\lambda^2\, G \iint A(x,y)\, T(x,y) \cos\left\{2\pi\left[s_x\,(x-\Omega t) + s_y\right] + \Psi\right\} dx\, dy. \qquad (11)$$

We assume that the antennas are made to track the source, so that $A(x,y)\, T(x,y)$ is not a function of t , and we make the following definitions:

$$A \equiv A(0,0)$$

$$AT'(x,y) \equiv A(x,y)\, T(x,y)$$

$$S' \equiv 2k/\lambda^2 \iint T'(x,y)\, dx\, dy \quad .$$

Then it can be shown that equation (11) may be written as

$$R(t) = GAS'V(s_x,s_y) \cos\left[\Phi(s_x,s_y) - 2\pi s_x \Omega t + \Psi\right] \quad , \qquad (12)$$

where V and Φ define the complex visibility function $\mathcal{V}(s_x,s_y)$ and are given by

$$\mathcal{V}(s_x,s_y) = V(s_x,s_y)\, e^{i\Phi(s_x,s_y)} = \frac{\iint T'(x,y)\, e^{i2\pi(s_x x + s_y y)} dx\, dy}{\iint T'(x,y)\, dx\, dy} \quad . \qquad (13)$$

The identity of equations (11) and (12) is evident if the sines and cosines are expressed in exponential form and coefficients of like terms are collected. It is seen that the visibility function is the complex, two-dimensional Fourier transform of T' , normalized to approach unity as s_x and s_y approach zero.

The procedure for measuring $T(x,y)$ with a two-element interferometer is one of measuring R , and hence V and Φ , at a sufficient number of values of s_x and s_y to determine the visibility function $\mathcal{V}$. The brightness temperature distribution can then be recovered by Fourier inversion of the visibility function. Inversion of $\mathcal{V}$ as defined above will actually produce T' , the source distribution modified by multiplication with $A(x,y)$, the antenna power pattern. For most discrete sources, $T(x,y)$ will be appreciably different from zero only within a region where $A(x,y) \approx A(0,0)$, in which case we also have $T(x,y) \approx T'(x,y)$ and $S \approx S'$. If this is not the case, $T(x,y)$

---

[2]We assume that for any "discrete" source $T(x,y)$ is non-zero only for values of x and y which are small enough that the approximations of equation (8) remain valid.

can be recovered from $T'(x,y)$ by dividing by $A(x,y)/A(0,0)$. If the source extends to regions where this ratio is very small, this procedure will introduce appreciable errors.

There remains the question of choosing suitable values of s_x and s_y for a given source. These depend on the overall extent of the source. Suppose the following condition holds:

$$T(x,y) = 0 \quad \text{whenever} \quad |x| > X \quad \text{or} \quad |y| > Y \ .$$

Then Bracewell (1958) has demonstrated that T is uniquely determined by the values of $\mathcal{V}$ at a lattice of points s_x and s_y such that

$$s_x = m/2X \quad , \quad s_y = n/2Y \quad , \tag{14}$$

where m and n are integers. Since $\mathcal{V}(-s_x,-s_y) = \mathcal{V}^*(s_x,s_y)$, observations need not be taken for negative values of one of the indices. Multiples of any spacings smaller than $1/(2X)$ and $1/(2Y)$ can be used, in which case the values of $\mathcal{V}$ will contain some redundancy.

How is the observer to arrange his baseline azimuths and spacings in order to sample the visibility function at the requisite points? The problem is simplified if all observations are made at transit. For observations on the local meridian, s_x is equal to the east-west component of the baseline, while s_y is equal to the north-south component foreshortened by the factor $\cos(\phi - \delta)$. Observations at the lattice points of equation (14) may be made with the interferometer elements placed at various equally-spaced locations on a tee-shaped track, as has been noted by Bracewell (1958).

Because the available range of antenna spacings is always limited, the visibility function is known only over a limited region. The recovery of the source brightness distribution is therefore not complete, since it lacks the fine detail contributed by the unknown Fourier components of high spatial frequency. The smoothing of a source distribution by omission of its high-frequency Fourier components has been discussed in detail by Bracewell and Roberts (1954). The resolution obtainable with finite apertures of different shapes has been discussed in the literature (see, for example, Covington and Harvey 1959; Ryle and Hewish 1960; Bracewell 1961).

c) Reduction to One Dimension

In many cases, observations are made with only a single baseline orientation. Such observations can only yield information about the distribution of source brightness in one dimension. They may be likened to observing the source with a fan beam, having high resolution in one dimension only. To see how this comes about, consider equation (13) with s_y set equal to zero and s_x equal to s,

$$\mathcal{V}(s,0) = V(s,0)e^{i\Phi(s,0)} = \frac{\iint T'(x,y)\, e^{i2\pi sx}\, dxdy}{\iint T'(x,y)\, dxdy} \ . \tag{15}$$

Let us define a one-dimensional brightness distribution $T'(x)$ by

integrating $T'(x,y)$ over y,

$$T'(x) \equiv \int T'(x,y)\, dy \quad .$$

Then if we define a one-dimensional visibility function $\mathcal{V}(s) \equiv \mathcal{V}(s_x,0)$, equation (15) becomes

$$\mathcal{V}(s) = V(s)\, e^{i\Phi(s)} = \frac{\int T'(x)\, e^{i2\pi sx}\, dx}{\int T'(x)\, dx} \quad . \qquad (16)$$

If $\mathcal{V}(s)$ is measured over a range of values of the antenna spacing s, its Fourier inversion will be an approximation to $T'(x)$.

Just as we can make a scan across a source with a fan beam oriented in any direction, so we can make a one-dimensional interferometric investigation using observations with an arbitrary baseline orientation. The direction of resolution is the direction in which the baseline is projected onto the source, i.e. that given by position angle p. No information is obtained about the distribution of the source normal to this direction.

One method of obtaining various baseline orientations with respect to a source is to observe the same source with the same physical baseline, but at varous hour angles. Equations (5) and (2) show that both the position angle p and the effective baseline $s\cos\theta$ will in general be changed at large hour angles. Some of the observations reported in this paper were made at large hour angles to take advantage of these changes.

It should be noted that two one-dimensional analyses with different baseline orientations (such as the east-west and north-south investigations reported in this and the following paper) do not constitute a full two-dimensional analysis. In terms of the visibility function, many of the essential lattice points given by equation (14) would be omitted in a set of measurements with only two baseline orientations. Nevertheless, some features of source structure may be established by such measurements. For instance, if a source contains two fairly well-separated centers of emission, measurements along two different axes allow the positions of the components to be determined. If the two components are identical, measurements along a third axis are necessary to remove the final ambiguity in their orientation.

d) Behavior of the Visibility Function at Small Spacings

It is of interest to consider the behavior of the visibility function in the region where the source is beginning to be resolved. For simplicity, we consider the one-dimensional case. If the exponential in equation (16) is expanded in powers of sx, we have for small s

$$V(s)\, e^{i\Phi(s)} = 1 + i2\pi s \frac{\int xT(x)\, dx}{\int T(x)\, dx} - 2\pi^2 s^2 \frac{\int x^2 T(x)dx}{\int T(x)dx} + i\tfrac{4}{3}\pi^3 s^3 \frac{\int x^3 T(x)dx}{\int T(x)dx} + \cdots \quad . \qquad (17)$$

If the origin is chosen at the centroid of the source, the first moment of the brightness distribution vanishes; hence, the departure of Φ from zero is cubic in s, while the departure of V from unity is quadratic and is proportional to the second moment of $T(x)$. If $V(s)$ is observed only in the region where it can be represented as

$$V(s) = 1 - U s^2 \quad ,$$

where

$$U \equiv 2\pi^2 \frac{\int x^2 T(x)\,dx}{\int T(x)\,dx} \quad ,$$

then it is clear that the second moment is the only feature of the source distribution which has been determined by the observations. Nevertheless, a "diameter" is often quoted for such a barely-resolved source, and this is customarily taken to be the diameter of the half-brightness contour in the circular Gaussian model which would have the same second moment as does the source.

III. OBSERVATIONS

The amplitudes, and in some cases the phases, of the complex visibility function have been measured for 127 discrete sources, using various spacings of up to 1557 wavelengths along an east-west baseline. The sources were selected mainly from the list of Harris and Roberts (1960), which will subsequently be referred to as CTA. Most of the CTA sources were, in turn, selected from the third Cambridge catalog (Edge, Shakeshaft, McAdam, Baldwin, and Archer (1959), which we designate 3C. Several galactic sources of relatively small diameter were selected from Wilson and Bolton's survey of the galactic plane (1960), which we will call CTB. A few additional sources from the 3C catalog or from the first catalog of Mills, Slee, and Hill (1958) were added to fill gaps in the observing program.

The Caltech interferometer has been described by Read (1961). The receiver used was a conventional superheterodyne, with a crystal mixer and an intermediate frequency preamplifier placed at the focus of each of the 90-ft paraboloids. Coherent local oscillator signals were supplied to the two mixers, and the IF signals were multiplied to produce the characteristic sensitivity pattern which has been given in equation (1). The receiver accepted radiation in both the signal and image bands, which were each about 5 Mc/s wide with a separation between centers of 20 Mc/s. All observations thus involve an average over these two bands. The local oscillator frequency was 958 Mc/s, corresponding to a wavelength of 31.3 cm, and all spacings have been calculated in terms of this wavelength.

At the time these observations were made, the available observing stations were at spacings of 200 ft, 400 ft, 800 ft, and 1600 ft east of a central base station. With one antenna at the central stations and the other at each of these stations successively, two series of observations were made: a primary series as the sources crossed the local meridian, and a secondary series at various distances east or west of the meridian.

a) Transit Observations

At each station, measurements were made of the apparent intensities and times of transit of the sources. For each source, the measurements taken at the different stations were compared to give information about the particular one-dimensional, complex visibility function which refers to position angle 90°.

To see how these measurements relate to the visibility function, consider equation (12), which gives the response of the interferometer to a discrete source. We repeat this equation, writing it in one-dimensional form as follows:

$$R(t) = GAS'V(s) \cos \left[\Phi(s) - 2\pi s\Omega t + \Psi \right] \quad .$$

At any antenna spacing, the apparent intensity of a source is given by $S'V(s)$. The visibility amplitude is obtained by dividing the apparent intensity by the true intensity. The true intensity, or flux, of the source may be obtained by extrapolation of the apparent intensities back to "zero" antenna spacing (since $V(0) \equiv 1$ -- cf. eg. (17)), or it may be obtained from total power measurements with a single antenna, such as the CTA or CTB measurements.

The apparent time of transit of a source is modified by the phase shift Φ . Most of the sources observed have diameters small enough that the phase can be normalized by assuming its value to be zero at the 195λ spacing. Thus the phase shifts for the longer spacings are given by

$$\Phi(s) = \frac{\alpha(s) - \alpha(195)}{\text{fringe period}} \times 360^\circ \qquad (18)$$

where $\alpha(s)$ is the apparent right ascension for observations at an antenna spacing of s wavelengths. Matthews (1961) has made available the right ascensions, measured at the 195λ spacing, for nearly all the sources observed. Therefore, the phases of the 195λ observations taken in the brightness distribution program were not reduced. For a few sources of large diameter, the phases were normalized to the CTA or CTB positions.

Table 1 summarizes the transit observations and gives the dates of each series. The coverage across the sky was not uniform, since most of the observations were taken at night. Of the total of 127 sources, the 79 lying between right ascensions 03^h and 19^h were particularly well covered.

TABLE 1

TRANSIT OBSERVATIONS

Station	Spacing	Fringe Period (min. of arc)	Dates (1960)
200 ft	195λ	17!66	25-29 Feb*
400 ft	389λ	8.83	30 Mar-4 Apr
800 ft	779λ	4.42	28 Apr-2 May
1600 ft	1557λ	2!21	15-20 May

*Observations made at this spacing were supplemented by observations made in June and October-November, 1960, by T. A. Matthews and others as part of a position-finding program.

b) Calibrations

The receiver gain was calibrated by observing, at each spacing, the three sources of very small diameter in the list published by Morris, Palmer, and Thompson (1957), namely 3C 147, 3C 196, and 3C 295. A fourth source, 3C 123, was used as a secondary standard. Its apparent intensity (compared to that of 3C 147) was reduced by no more than 3% at the 1557λ spacing.

A complete knowledge of the receiver gain variations could not be obtained from observations of only these four small sources. Among all the sources observed, there were a number with sufficient strength that their apparent intensities were unaffected by noise fluctuations. Since all sources should have a constant apparent intensity at a given spacing, any variations from night to night in the intensities observed for the strong sources could be attributed to gain variations. By adjusting the gain calibration factor G to give both constant intensities for the strong sources at a given spacing and constant intensities for the small sources at all spacings, the uncertainty in gain was reduced. All apparent intensities were corrected for the attenuation of the output time constant in the receiver.

The phase calibrations were made only after the amplitude calibrations were complete. About half the sources were only slightly resolved at the longest spacing. These sources would be expected to show no phase shifts, and all were used as calibrators to determine the variations in the instrumental phase shift Ψ throughout each night of observation. The apparent times of transit were corrected for the effects of precession, aberration, and nutation and for the delay of the output time constant.

c) Off-Transit Observations

Since the number of effective spacings available at transit was rather small, a second set of observations of the sources was made at each station, at various distances from the meridian. The purpose of these was to take advantage of the foreshortening of the baseline which occurs when a source is observed at large hour angles.

As can be seen from equation (6), this foreshortening is accompanied by a rotation of the interference fringes with respect to the source. For an east-west baseline, the angle of rotation is $p-90^\circ$. This rotation is very much a function of declination, and it could be neglected for many sources having $|\delta| < 15^\circ$. For such sources, the off-transit observations yielded values of the east-west visibility amplitude at additional antenna spacings. No attempt was made to recover the visibility phase in the off-transit observations.

For sources with large absolute declinations, the off-transit observations yielded information about the brightness distribution in the north-south direction. More precisely, a set of observations of a source at a given hour angle, but taken at the different observing stations, yielded values of the amplitude of a one-dimensional visibility function with resolution along an axis in position angle p. Although the associated phases were not measured, their general behavior could sometimes be inferred from the behavior of the amplitudes and from the results of the transit observations. For some sources these measurements in different position angles proved very useful. They were particularly useful for determining the orientation of the major axis of an elongated source.

On any one night, sources were observed at a constant value of the effective spacing, i.e. a constant value of the angle θ -- which we may call θ_o . For a fixed value of θ_o , the hour angle is given as a function of declination by the relation,

$$\sin h = - \sin \theta_o \sec \delta \quad . \tag{19}$$

Since the hour angle coverage was limited by the antenna mountings and by the surrounding terrain, sources outside a certain declination range could not be observed at a given effective spacing.

Table 2 gives the particulars of the off-transit observations. In each set, measurements were made both east and west of the meridian in order to obtain the two possible values of the position angle p . For purposes of analysis, the two sets of measurements taken at the 200 ft station were grouped with the sets taken at 800 ft and 1600 ft which have nearly the same two values of $\cos \theta_o$. For all off-transit observations, the path lengths traversed by the signals from the two antennas were equalized by adding cable with an electrical length of $s \sin \theta_o$ to the IF lead coming from whichever antenna was nearer to the source.

TABLE 2

OFF-TRANSIT OBSERVATIONS

Station	$\cos \theta_o$	Effective Spacing	Dates (1960)	No. of Nights	
				E	W
200 ft	0.646	126λ	2-4 Mar	1	1
	0.867	169λ	29 Feb-2 Mar	1 1/2	1 1/2
400 ft	0.750	292λ	4-9 Apr	2	2
800 ft	0.625	487λ	7-9 May	1	1
	0.750	584λ	2-5 May	1	2
	0.875	681λ	5-7 May	1	1
1600 ft	0.625	973λ	24,27-29 May	2	1
	0.750	1168λ	19-24 May	2	2
	0.788	1226λ	29 May	1/2	1/2
	0.875	1363λ	25-27 May	1	1

Table 3 gives the declination limits for the three principal values of $\cos \theta_o$.

TABLE 3

DECLINATION LIMITS

$\cos \theta_o$	δ
0.625	-38° to $+55^\circ$
0.750	-32 to +40
0.875	-25 to +25

The amplitudes of the off-transit observations were analyzed in the same way as those of the transit observations, using the same sources as calibrators. There was no indication that any of the calibrators had an appreciable north-south diameter[3]. For measurements with $\cos \theta_o = 5/8$, none of the four calibrators were within the available declination range. Values of the apparent intensities of 3C 161 and 3C 273 were interpolated from the transit measurements and used to calibrate these observations. Both of these are moderately intense, small sources located near the celestial equator.

d) Errors

Errors in the visibility amplitudes were mainly caused by receiver gain variations and by receiver noise fluctuations. The uncertainty in the receiver gain calibration could be estimated from the consistency of all the data taken at a single spacing. The estimate of this error varied from 3% for the best sets of transit data to about 10% for some of the off-transit data. The noise fluctuations were equivalent in amplitude to the interference pattern produced by a source with an apparent intensity of between 0.4 and 0.8×10^{-26} W $m^{-2}(c/s)^{-1}$.

The rms error in the visibility amplitude has been estimated for each observation taken at transit and at the 1168λ effective spacing. These estimates are given along with the visibility amplitudes in Tables 4 and 7. Individual estimates of errors are not tabulated for the other off-transit observations, but they may be obtained from the following formula:

$$\text{rms error in } V \approx \left[(0.6/S)^2 + (0.1V)^2\right]^{1/2} ,$$

where V is the tabulated amplitude and S is the flux for the source as given in Table 4. This formula assumes a gain uncertainty of 10% and an intensity error due to noise of 0.6×10^{-26} W $m^{-2}(c/s)^{-1}$.

[3]The north-south diameter of 0!5 which Maltby (1962) finds for 3C 123 is just consistent with this result.

For all but the very weakest sources, the errors in the phase of the visibility function were dominated by the uncertainty in the calibration of the instrumental phase shift. An estimate was made of the error in each phase observation, and these estimates are included in Table 5.

Errors due to confusion set a lower intensity limit on any investigation of discrete sources. In the present observations there was an average of one source per primary beam area at an intensity level of about 0.3×10^{-26} W $m^{-2}(c/s)^{-1}$, or about the level of the noise fluctuations. This estimate is based on the density of faint sources reported in a recent Cambridge survey (Leslie 1961) and is roughly confirmed by our own observations. Only nine sources observed with the east-west baseline had intensities of less than 3×10^{-26}, with the faintest having an intensity of 1.2×10^{-26}. Only for these sources should the confusion effects be at all serious. They are 3C 28, 3C 46, 3C 135, 3C 191, 3C 243, MSH 19-16, 3C 413, and 3C 469.

IV. VISIBILITY FUNCTIONS

In Tables 4-9 are presented data on the visibility functions of the 127 sources which were observed with the east-west baseline. The visibility amplitudes for 51 sources are plotted in Figures 2-8. These latter sources have been chosen because their visibility functions are reasonably complete and show interesting features. Generally this means that these sources have major structural features with characteristic angular sizes of between 1!5 and 15'. The detailed interpretation of this information will be given in the third paper of this series.

Table 4 includes all the sources, and in it are given the visibility amplitudes, as observed at the four transit spacings, and the source intensities, or fluxes. For sources included in the CTA or CTB lists, a visibility amplitude at "zero spacing" is also given. This zero-spacing amplitude is equal to the CTA or CTB intensity divided by the intensity of Table 4. In most cases this ratio is unity, within the error of measurement, but there are some exceptions. In a case where this ratio is larger than unity, the source may possibly have a broad emission feature which was completely resolved by the interferometer at the smallest spacing available.

The intensities have been determined by comparison of the east-west interferometer data, the CTA and CTB data, and the north-south interferometer data obtained by Maltby. All intensities are based on an assumed value for the flux from M87, at 31.3 cm, of 300×10^{-26} W $m^{-2}(c/s)^{-1}$, which is the same value assumed in preparing the CTA and CTB lists. A recent re-evaluation by Wilson (1961) of the published data on absolute flux measurements suggests that this assumed value is about 3% too high. In the few cases where this change would be significant, the intensities in Table 4 may be scaled accordingly. Since the correction is small and still somewhat uncertain, it was not thought worthwhile to revise Table 4.

The intensities have been corrected for atmospheric extinction and are the values which would be observed if no atmosphere were present. A value of 0.0076 was assumed for the 31.3 cm sea-level extinction at the zenith.

For a source with a large diameter, the apparent intensities observed with the interferometer cannot be extrapolated back to zero spacing to give

the total flux. For such sources, the CTA or CTB intensity (corrected for extinction) has been adopted, and these are indicated by an intensity value enclosed in parentheses. Wilson (1961) has provided improved estimates of the intensities of several of the CTB sources. Some sources were large enough to be partially resolved by the primary antenna beam; for these sources the peak apparent intensity is tabulated, and these are marked with a dagger. Three sources for which fluxes are given in Table 4, namely 3C 17, 3C 28, and 3C 41, were observed only off-transit.

A source marked with an asterisk is one for which the visibility amplitude is plotted in Figures 2-8. A visibility amplitude based on only one observation is marked with a colon. The sources are identified either by familiar names of long standing, or by their numbers in the 3C, CTA, or CTB surveys or in the first survey of Mills, Slee and Hill (1958). "Coma A" is the source so designated in the Jodrell Bank survey of the region containing the Coma cluster of galaxies (Large, Mathewson, and Haslam 1959).

Table 5 gives the visibility phases for the transit observations. Unless otherwise noted, they are normalized to Matthews' 195λ positions in the way indicated by equation (18). About half the sources observed were virtually unresolved at the longest available spacing. These sources would be expected to have no appreciable phase shift, and the method of calibration assumed that this was so. In Table 5 are listed only those sources for which the phase was measured and found to be significantly different from zero at one or more spacings. Phases were measured for all source-spacing combinations for which an amplitude (not an upper limit) is entered in Table 4, except for the following: 3C 40, 3C 58, and 3C 66 at 389λ; CTA 26 at 1557λ; 3C 280 at 779λ; 3C 298 at 1557λ; 3C 380 at 779λ; and MSH 19-16, CTB 87, CTA 97, and 3C 469 at all spacings.

The convention as to the sign of the phase is given by the definitions in Section II. A positive phase shift corresponds to an apparent displacement of the source toward the east. Again in Table 5, a colon denotes a value based on a single observation.

In Tables 6-9 are listed the visibility amplitudes measured in the off-transit observations. The direction of resolution, or the direction of the baseline when projected against the sky, is defined by the position angle p. For observations of the same source at a given value of $\cos\theta_o$, but on opposite sides of the meridian, p differs from 90° by the same amount but in opposite senses (c.f. eq. (6)). The value of $|p-90^\circ|$ is tabulated for each source and each value of $\cos\theta_o$. The rules for determining p are as follows:

$$p > 90^\circ \quad \text{for} \quad \delta > 0, \quad h < 0 \quad \text{or for} \quad \delta < 0, \quad h > 0;$$

$$p < 90^\circ \quad \text{for} \quad \delta > 0, \quad h > 0 \quad \text{or for} \quad \delta < 0, \quad h < 0.$$

The observations taken east and west of the meridian have been averaged for some sources located near the celestial equator; for these sources the fringe rotation angle $|p-90^\circ|$ was small. Such averages are marked with an A. Except for these averages, and except for many of the observations made with the 1168λ effective spacing, most of the entries in Tables 6-9 are the result of single observations.

In Figures 2-8 the visibility amplitudes for 51 sources are plotted. In the graphs, the filled circles refer to transit observations, while the open circles refer to off-transit observations. Unless otherwise noted, all curves are of one-dimensional visibility amplitudes with resolution in position angle 90°. Open circles appearing on the position angle 90° curves represent off-transit observations for which the effect of the fringe rotation was judged to be negligible. Some off-transit points, particularly those for which the effects of the fringe rotation are not clear, have been omitted from the graphs. A dashed line indicates that the behavior of the visibility function in that region is not well determined by the available data.

A striking feature of the visibility curves in Figures 2-8 is their general complexity. Many show peaks and valleys, which are associated with a complex source-structure, while only a few show a smooth decline of amplitude with increasing spacing, which is the signature of a simple type of source. This tendency towards complexity in the sources is examined in detail in the third paper in this series (Maltby and Moffet 1962), in which the east-west and the north-south visibility functions are interpreted in terms of the structure of the sources.

V. ACKNOWLEDGMENTS

The material in this paper forms a portion of a thesis submitted to the Faculty of the California Institute of Technology in partial fulfillment of the requirements for the Ph.D. degree. The author has held a National Science Foundation Predoctoral Fellowship during the cource of this work. The assistance of D. Morris, V. Radhakrishnan, and D. E. Harris in taking the observations is gratefully acknowledged, as are the discussions and criticisms of P. Maltby, T. A. Matthews, R. B. Leighton, G. J. Stanley, and J. G. Bolton. Thanks are due to Matthews and to R. W. Wilson for making available the results of their observations in advance of publication.

The program in radio astronomy at the California Institute of Technology is supported by the United States Office of Naval Research under Contract Nonr 220(19).

APPENDIX

We desire an expression for $\sin\theta$ in terms of hour angle and declination. Referring to Figure 9, let N be the north celestial pole, Z the local zenith, ϕ the geographic latitude, and Q the position of the source at hour angle h and declination δ. Point P is the interferometer pole, i.e. the intersection of the extended baseline with the unit sphere, and is determined by the azimuth α.

Let **i**, **j**, and **k** be unit vectors of a Cartesian system with **k** pointing towards the local zenith and **i** and **j** in the local horizontal plane as shown. Another system **i'**, **j'**, and **k'** is rotated with respect to the first so that **k'** points at N. The unit vector along the baseline is

$$\mathbf{e}_P = -\mathbf{i}\cos\alpha + \mathbf{j}\sin\alpha \quad ,$$

while that in the direction of the source is

$$\mathbf{e}_Q = \mathbf{i}'\cos\delta\cos h - \mathbf{j}'\cos\delta\sin h + \mathbf{k}'\sin\delta \quad .$$

But we may express **i'**, **j'**, and **k'** as

$$\mathbf{i}' = \mathbf{i}\sin\phi + \mathbf{k}\cos\phi \quad ,$$

$$\mathbf{j}' = \mathbf{j} \quad ,$$

$$\mathbf{k}' = -\mathbf{i}\cos\phi + \mathbf{k}\sin\phi \quad .$$

Then $\mathbf{e}_Q$ becomes

$$\mathbf{e}_Q = \mathbf{i}(\sin\phi\cos\delta\cos h - \cos\phi\sin\delta) - \mathbf{j}\cos\delta\sin h + \mathbf{k}(\cos\phi\cos\delta\cos h + \sin\phi\sin\delta),$$

and $\mathbf{e}_P\cdot\mathbf{e}_Q = \cos(\pi/2-\theta) = \sin\theta$ may be written as

$$\sin\theta = -\sin\alpha\cos\delta\sin h + \cos\alpha(\cos\phi\sin\delta - \sin\phi\cos\delta\cos h) \quad .$$

REFERENCES

Bracewell, R. N. 1958, Proc. Inst. Radio Engrs., 46, 97.

_____. 1961, Trans. Inst. Radio Engrs., AP-9, 59.

Bracewell, R. N., and Roberts, J. A. 1954, Australian J. Phys., 7, 615.

Covington, A. E., and Harvey, G. A. 1959, Can. J. Phys., 37, 1216.

Edge, D. O., Shakeshaft, J. R., McAdam, W. B., Baldwin, J. E., and Archer, S. 1959, Mem.Roy. Astron. Soc., 68, 37.

Harris, D. E., and Roberts, J. A. 1960, Pub.A.S.P., 72, 237.

Large, M. I., Mathewson, D. S., and Haslam, C.G.T. 1959, Nature, 183, 1664.

Leslie, P. R. R. 1961, M.N., 122, 51.

Maltby, P. 1962, submitted to Ap.J.

Maltby, P., Matthews, T. A., Moffet, A. T. 1962, submitted to Ap.J.

Maltby, P., and Moffet, A. T. 1962, submitted to Ap.J.

Matthews, T. A. 1961, private communication.

Michelson, A. A. 1890, Phil. Mag., 30, 1.

_____. 1891, Phil. Mag., 31, 256.

_____. 1920, Ap.J., 51, 257.

Michelson, A. A., and Pease, F. G. 1921, Ap.J., 53, 249.

Mills, B. Y., Slee, O. B., and Hill, E. R. 1958, Australian J. Phys., 11, 360.

Morris, D., Palmer, H. P., and Thompson, A. R. 1957, Observatory, 77, 163.

Read, R. B. 1961, Trans. Inst. Radio Engrs., AP-9, 31.

Ryle, M. 1952, Proc. Roy. Soc.(London) A, 211, 351.

Ryle M., and Hewish, A. 1960, M.N., 120, 220.

Wilson, R. W. 1961, private communication.

Wilson, R. W., and Bolton, J. G. 1960, Pub. A.S.P., 72, 331.

TABLE 4

FLUXES AND VISIBILITY AMPLITUDES FOR TRANSIT OBSERVATIONS

Source	Flux	Spacing				
		0	195λ	389λ	779λ	1557λ
3C 2	5.1±0.4	---	0.87±.17:	---	---	1.00±.10
SN 1572*	(57±3)	1.00±.05	0.69±.07	---	0.17±.02:	0.08±.01:
3C 15	5.5±0.4	0.93±.21	1.07±.15:	---	---	---
3C 17	7.8±0.5	1.30±.30	---	---	---	---
3C 20	14.7±1.8	0.93±.11	0.92±.15:	---	0.90±.08:	0.80±.08:
3C 26	3.2±0.6	---	0.92±.15	---	0.97±.15	1.06±.20:
3C 28	2.7±0.3	0.89±.33	---	---	---	---
3C 33*	18.6±0.9	0.97±.03	0.86±.10:	0.84±.07:	0.64±.06:	0.35±.05:
3C 38	7.0±0.7	1.19±.22	0.64±.11	---	---	0.65±.10:
3C 40*	8.0±1.2	1.00±.22	0.81±.12	0.29±.05:	0.49±.07:	0.11±.05:
3C 41	(6.9±0.9)	1.00±.13	---	---	---	---
3C 46	2.2±0.5	---	1.11±.15:	0.75±.14:	0.42±.22:	---
3C 48	21.5±1.1	0.98±.08	---	---	---	1.00±.07
3C 58*	35.0±2.4	0.95±.05	0.63±.06:	0.36±.03:	0.08±.01:	0.06±.01
3C 63	5.3±0.8	1.15±.19	0.91±.16	---	---	---
3C 66*	(12.9±0.9)	1.00±.08	0.46±.10:	0.46±.06:	0.20±.04:	0.20±.02
MSH 02-110	6.4±0.4	---	1.04±.16	---	---	---
3C 71	6.9±0.3	---	0.82±.14:	---	0.95±.11:	0.91±.06
3C 75*	8.1±0.4	0.92±.07	0.81±.13:	0.72±.12:	0.11±.06:	0.31±.07
3C 78	9.1±1.4	---	0.88±.13:	---	0.76±.10:	---
3C 79	7.0±0.5	0.97±.08	---	0.90±.18:	0.88±.12:	0.36±.04
CTA 21	9.3±0.7	0.97±.11	0.89±.10	---	---	---
NGC 1275*	20.4±2.0	1.05±.11	0.90±.09	0.88±.05:	0.77±.05:	0.71±.04
Fornax A	(125±6)†	1.00±.04	0.05±.01:	0.03±.01:	0.01±.00:	---
3C 89*	(6.3±0.9)	1.00±.16	0.59±.09	0.70±.09:	0.63±.08:	0.47±.08:
CTA 26	2.8±0.4	1.25±.41	0.77±.22:	---	0.79±.17:	0.69±.21
3C 98*	(14.1±1.2)	1.00±.08	0.92±.04	0.88±.10	0.55±.05:	0.33±.03
3C 103	7.2±0.5	0.92±.08	0.97±.05:	---	0.99±.12:	0.99±.11:
3C 109	5.9±0.6	0.86±.16	0.92±.05	0.96±.09:	0.97±.09:	---
3C 111*	20.4±2.0	1.00±.08	0.89±.04:	0.69±.04:	0.07±.03:	0.33±.05
3C 123	64.3±1.9	1.05±.03		standard source		
3C 129*	10.6±1.1	0.89±.11	0.46±.02	0.48±.03	0.23±.03	0.31±.03
3C 134*	15.1±0.8	1.00±.08	0.99±.04:	1.01±.04	0.90±.06:	0.81±.03
3C 135	2.9±0.9	---	0.83±.15:	0.57±.11:	---	0.66±.17:
Pictor A*	(86.8±2.6)	1.01±.07	0.54±.03:	0.06±.01:	0.17±.01:	0.09±.01:
Crab Neb.*	(1030±45)	1.00±.04	0.92±.06	0.64±.02	0.14±.01:	0.04±.00:
Orion Neb.*	(361±9)	1.00±.03	0.64±.03	0.31±.02:	0.11±.01:	0.02±.00:
3C 147	29.2±0.9	0.99±.03		standard source		
3C 154	7.2±0.5	0.95±.08	0.99±.05	0.97±.06	0.87±.09	0.80±.08:
3C 161	25.6±1.3	0.93±.06	1.00±.05	0.97±.05	1.00±.06	0.97±.05:
3C 171	5.7±0.4	1.05±.16	0.95±.05	0.97±.08	1.00±.10	0.92±.19:
3C 175	4.1±0.4	---	0.94±.09	0.98±.05	0.96±.05	0.69±.13:
3C 180	4.3±0.6	---	0.94±.11	1.00±.09	0.98±.07	0.75±.14:
3C 191	2.9±0.4	---	1.01±.11	0.98±.15	0.97±.15	1.19±.33:
3C 196	20.4±0.8	1.03±0.8		standard source		

TABLE 4 Continued

Source	Flux	Spacing				
		0	195λ	389λ	779λ	1557λ
3C 198*	3.4±0.3	---	0.92±.07	0.73±.10:	0.27±.14:	0.30±.13:
Puppis A	(105±6)†	1.00±.06	0.13±.02:	0.02±.01:	0.01±.00:	---
3C 208*	4.9±1.2	---	0.83±.06	0.57±.08	1.03±.11:	0.99±.10
CTB 31*	(212±21)†	1.00±.10	0.48±.04:	0.40±.02:	0.20±.01:	0.04±.00:
CTB 32*	(34.3±5)†	1.00±.15	0.74±.08:	0.52±.02:	0.23±.02:	---
3C 216	6.0±0.4	---	0.95±.05	1.03±.05	1.01±.11:	0.96±.11:
Hydra A*	(67.5±1.8)	1.00±.03	0.97±.04	0.95±.04	0.83±.03	0.71±.02
3C 219*	12.3±0.9	---	0.95±.05	0.91±.04	0.67±.06:	< 0.10:
3C 227*	11.2±1.1	0.91±.09	0.83±.05	0.69±.05	0.22±.02	0.11±.03
3C 230	5.9±0.4	---	0.85±.07:	0.77±.10	0.70±.13:	0.84±.11:
3C 234*	8.3±0.8	0.88±.12	1.00±.04	0.65±.04	0.62±.05	0.43±.08
3C 237	9.6±0.7	0.57±.10	1.01±.08:	1.00±.04	0.86±.10:	0.99±.11
3C 243	2.1±0.5	---	---	0.67±.11	0.61±.15	0.56±.22
3C 254	5.1±0.4	---	0.99±.06	1.02±.05	0.95±.08	0.99±.06
3C 264*	(10.5±3.0)	1.00±.29	0.72±.06	0.59±.05	0.47±.06	0.31±.05
3C 265	4.8±0.5	---	0.95±.08	0.86±.09	0.72±.10:	0.37±.10:
3C 270*	(28.5±1.5)	1.00±.05	0.56±.03	0.07±.01	0.23±.02	0.08±.02
3C 273	45.4±1.4	1.11±.05	1.00±.04	1.00±.03	0.97±.05	0.94±.04:
M 87*	300 ---	1.00±.05	0.84±.03	0.59±.02	0.50±.02:	0.38±.01
Coma A	4.0±0.6	---	---	0.89±.13:	1.12±.15:	0.98±.24
3C 278*	10.6±1.1	0.91±.15	0.94±.13:	0.74±.06:	0.42±.05:	< 0.15:
3C 279	9.8±0.7	0.70±.12	1.01±.08	0.99±.08:	0.82±.10:	0.92±.10:
3C 280	7.2±0.7	0.95±.16	0.96±.06:	1.02±.08:	0.93±.12:	0.90±.09:
3C 283	8.6±0.9	1.18±.18	0.98±.04	1.01±.09	0.97±.06	0.83±.08
NGC 5128*	(442±35)†	1.00±.07	0.53±.02:	0.15±.01	0.33±.01	0.08±.01
3C 286	19.8±1.4	0.99±.08	0.99±.05:	1.03±.05:	1.00±.05:	1.02±.06:
3C 287	9.6±0.9	0.88±.13	0.85±.05	1.09±.08:	0.95±.10:	0.91±.09:
3C 295	32.0±1.0	0.95±.07		standard source		
3C 298	9.7±0.5	1.15±.16	0.97±.05	1.07±.06:	1.05±.09:	0.94±.05
MSH 14+010	3.4±0.7	---	0.85±.12:	0.64±.11	0.81±.16	0.70±.19
3C 310*	12.7±0.9	0.85±.14	0.98±.07:	0.89±.06	0.60±.06	0.17±.04
3C 313*	6.0±0.9	0.91±.16	0.85±.15:	0.85±.09:	0.43±.06:	0.62±.17
3C 315	6.1±0.6	1.00±.16	0.97±.05:	0.94±.09:	0.87±.06	0.52±.06
3C 317	10.0±0.7	1.00±.10	1.00±.10:	0.97±.07:	0.96±.06:	0.93±.06
3C 318	4.1±0.6	0.72±.24	0.97±.20:	0.94±.07	1.03±.06:	1.04±.18:
3C 324	4.2±0.6	1.50±.37	0.88±.08	0.93±.06	0.91±.07	0.98±.16
3C 327*	12.3±1.2	0.95±.17	0.91±.04	0.63±.09	0.58±.06	0.28±.04
MSH 16+02	6.5±1.0	---	0.94±.14	---	0.97±.10:	0.68±.26
3C 330	10.6±0.7	0.83±.15	0.99±.06	0.93±.08	0.82±.05	0.35±.04
3C 338*	6.7±0.5	1.08±.17	0.97±.06	0.93±.05	0.78±.04	0.38±.05
3C 343*	(10.5±0.9)	1.00±.09	0.32±.02	0.98±.06:	0.17±.02:	0.85±.07:
3C 345	8.4±0.8	1.00±.14	0.95±.08:	0.98±.07	0.96±.09:	0.82±.07:
3C 347*	2.5±0.6	---	0.96±.12:	0.54±.20:	0.59±.11:	0.88±.20:
Herc A*	73.5±3.7	1.00±.08	0.93±.03:	0.76±.03:	0.27±.01	0.61±.02
CTB 38	(38±13)†	1.00±.30	0.56±.06:	0.59±.03:	0.18±.03	0.08±.02:

TABLE 4 Continued

Source	Flux	Spacing				
		0	195 λ	389 λ	779 λ	1557 λ
3C 353*	81.5±1.8	1.04±.02	0.88±.03	0.61±.02	0.27±.01	0.25±.01
SN 1604*	21.3±2.1	0.95±.10	0.97±.08	0.84±.07	0.41±.02	0.19±.02
Sgtr A*	(700±140)†	1.00±.20	0.30±.06:	---	0.07±.00	0.02±.00
3C 365	3.5±0.5	---	1.03±.12:	---	0.78±.12	0.98±.07
Omega Neb.*	(502±75)†	1.00±.15	0.55±.04:	0.26±.01	0.05±.00	0.02±.00
3C 380	19.8±1.0	0.93±.03	0.98±.12:	1.00±.05:	1.00±.05:	1.02±.04
CTA 80*	7.8±0.8	0.88±.07	1.00±.12:	0.75±.07:	0.52±.07	0.38±.06:
3C 386*	10.2±0.5	0.94±.06	---	0.87±.07:	0.64±.04	0.17±.05:
3C 388	(9.9±1.2)	1.00±.12	0.86±.10:	0.81±.05	0.90±.07	0.69±.08
3C 397*	(25±13)†	1.00±.50	0.53±.07:	0.36±.02	0.13±.03	0.10±.06
3C 398*	(92±14)†	1.00±.15	0.45±.07	0.19±.01:	0.08±.01	0.06±.01
MSH 19-16	1.2±0.4	---	0.95±.35:	---	0.82±.22	1.12±.60
3C 401	7.2±0.5	1.09±.14	---	1.00±.07:	0.99±.08	1.01±.09:
3C 402*	4.9±1.0	0.92±.24	0.90±.15	---	0.43±.05:	0.35±.07:
3C 403*	(9.6±0.6)	1.00±.06	0.71±.13:	---	0.47±.05:	0.25±.04
Cygnus A	(2160±120)	1.00±.06	---	---	0.49±.03	0.41±.02
3C 409	21.0±1.5	1.05±.06	---	---	0.98±.05	1.00±.10
CTB 87	(10.0±4.0)†	1.00±.40	0.81±.12:	---	0.11±.03:	0.27±.08:
3C 410	12.7±0.9	1.02±.08	---	---	0.98±.05	0.93±.06
3C 413*	1.5±0.4	---	0.95±.20:	---	0.41±.11	0.62±.37:
3C 424	3.9±0.4	1.60±.25	0.98±.09	---	0.94±.08	1.09±.16
3C 430	11.2±1.1	1.00±.14	1.00±.10:	---	---	0.75±.10:
3C 433	17.4±0.9	0.89±.09	---	---	0.93±.04	0.93±.04
3C 436	(6.3±0.6)	1.00±.10	0.81±.13:	---	0.76±.07	0.77±.09
CTA 97	(4.5±0.6)	1.00±.13	0.29±.07:	---	---	---
3C 438	10.6±0.5	1.00±.06	1.08±.15:	---	0.97±.05	1.06±.09
3C 444	13.6±0.7	1.00±.04	---	---	0.92±.05	0.79±.09
3C 445*	(8.2±1.2)	1.00±.14	0.95±.11	---	0.59±.07:	0.16±.05:
3C 446*	(7.8±0.9)	1.00±.12	0.96±.12	---	0.74±.10:	1.01±.09
CTA 102	7.8±0.5	0.93±.08	---	---	1.00±.12:	0.99±.15
3C 452*	15.3±1.5	0.91±.06	0.86±.08	---	0.09±.02:	0.10±.01
3C 456*	3.4±0.9	---	1.05±.15:	---	0.73±.10:	1.00±.16
3C 459	(7.2±0.6)	1.00±.08	---	---	0.94±.11:	0.82±.10
Cass A	(3120±150)	1.00±.05	---	---	0.08±.01:	0.06±.00
MSH 23-112	3.2±0.5	---	1.00±.18:	---	0.97±.16:	0.86±.08
3C 465*	(11.7±0.9)	1.00±.08	0.78±.10	---	0.26±.05:	0.37±.07
3C 469	2.3±0.6	---	0.60±.25	---	---	0.62±.10

Notes-- All fluxes are given in units of 10^{-26} w m^{-2} $(c/s)^{-1}$
* Amplitudes for these sources are plotted in figures 2-8
( ) CTA or CTB flux
† Peak apparent flux from CTA or CTB
: Based on a single observation

TABLE 5

VISIBILITY PHASES FOR TRANSIT OBSERVATIONS

Source	Spacing		
	389λ	779λ	1557λ
SN 1572	---	+170° ± 30°	+70° ± 50°
3C 33	---	00 ± 30:	-120 ± 50:
3C 40	---	+130 ± 30:	+180 ± 60:
3C 58	---	-70 ± 50:	-75 ± 50:
3C 66	---	-120 ± 30:	-230 ± 50:
3C 75	00° ± 20°	-70 ± 30:	-155 ± 40:
Fornax A (1)	+110 ± 20:	-60 ± 40:	---
3C 89	+20 ± 20:	+25 ± 40:	+85 ± 70:
3C 98	00 ± 15	+25 ± 20:	+210 ± 40:
3C 111	00 ± 15:	-50 ± 40:	-170 ± 40:
3C 129	+45 ± 20	+90 ± 30	+250 ± 80
3C 135	+30 ± 20:	---	+235 ± 80
Pictor A	-120 ± 20:	-40 ± 20:	---
Crab Neb.	00 ± 10	00 ± 10:	+90 ± 30:
Orion Neb.	00 ± 10:	-20 ± 10:	-140 ± 30:
Puppis A	+115 ± 10:	00 ± 40:	---
3C 208	-40 ± 20	-90 ± 30:	-120 ± 30
CTB 31 (2)	-20 ± 20:	+15 ± 30:	+70 ± 40:
CTB 32 (2)	-50 ± 20:	-90 ± 30:	---
Hydra A	+10 ± 10	+40 ± 15	+90 ± 40
3C 227	+10 ± 20	+110 ± 30	+230 ± 70
3C 270	-95 ± 10	-125 ± 30	-270 ± 40
M 87	+10 ± 10	+25 ± 30:	+80 ± 40
3C 278	+25 ± 20:	+50 ± 20:	---
NGC 5128	+145 ± 20	+185 ± 15	+550 ± 40
3C 287	+45 ± 20:	+90 ± 30:	+170 ± 40:
3C 313	00 ± 15:	00 ± 30:	-115 ± 50
3C 327	+30 ± 20	+155 ± 15	+280 ± 40
3C 343	-90 ± 20:	-50 ± 30:	-30 ± 40
3C 347	+120 ± 20:	+180 ± 40:	+510 ± 60:
Herc A	+10 ± 10:	+50 ± 15	+190 ± 30
CTB 38 (2)	-15 ± 20:	-140 ± 30	-290 ± 50:
3C 353	+10 ± 10	+130 ± 15	+230 ± 30
SN 1604	00 ± 10	+50 ± 20	-70 ± 30
Sgtr A (2)	---	-10 ± 20	-200 ± 30
Omega Neb.	-15 ± 10	-45 ± 15	- 90 ± 30
CTA 80	+40 ± 10:	+10 ± 20	+160 ± 60:
3C 397	-70 ± 20:	+140 ± 20	-140 ± 40
3C 398	-135 ± 20:	-170 ± 20	-300 ± 60
3C 402	---	+65 ± 40:	+190 ± 80:
3C 403	---	+60 ± 30:	+290 ± 50
Cyg A	00 ± 10:	+10 ± 10	+150 ± 30
3C 413	---	-50 ± 40	-280 ± 60:
3C 452	---	+140 ± 50:	+30 ± 40
Cass A	---	-65 ± 20:	+90 ± 30

TABLE 5 Continued

Source	Spacing		
	389λ	779λ	1557λ
3C 465	---	$+115^{\circ} \pm 40^{\circ}$:	$+230^{\circ} \pm 50^{\circ}$

Notes-- Only those sources are listed which have phases differing significantly from zero.
: based on a single observation
(1) normalized to the CTA position
(2) normalized to the CTB position

TABLE 6

VISIBILITY AMPLITUDES FOR OBSERVATIONS WITH $\cos \theta_o = 5/8$

Source	Effective Spacing						$\lvert p-90^{\circ} \rvert$
	126		487		973		
	E	W	E	W	E	W	
3C 2	--	--	0.94	—	0.95	--	00
3C 15	--	--	--	--	0.70	--	02
3C 26	--	0.86	--	--	--	--	03
3C 33	--	--	0.87	--	0.87	--	16
3C 38	--	--	--	--	0.78	--	19
3C 40	--	0.95	0.44	--	< 0.15	--	02
3C 63	--	0.96	--	--	0.96	--	03
3C 75	--	0.93	--	--	0.15	--	07
3C 79	--	--	--	--	0.53	--	05
CTA 21	--	0.89	--	--	0.95	--	21
3C 89	--	--	--	--	0.40	--	02
CTA 26	--	--	--	--	0.88	--	03
3C 98	--	0.93	--	0.65	--	--	12
3C 109	--	0.94	--	1.06	--	--	13
3C 135	--	0.98	--	0.62	--	--	02
Crab Neb.	--	0.93	--	0.65	--	0.14	28
Orion Neb.	--	--	--	0.21	--	0.05	07
3C 154	--	1.00	--	--	--	--	35
3C 175	0.84	0.95	--	0.96	--	0.85	14
3C 180	1.02	--	--	--	--	--	03
3C 191	1.11	0.99	--	--	--	--	12
3C 198	0.99	0.81	--	0.56	--	--	07
3C 208	0.75	1.19	--	0.57	--	0.93	16
Hydra A	1.00	1.02	--	--	--	0.74	14
3C 227	--	0.98	--	--	--	0.24	09

TABLE 6 Continued

Source	Effective Spacing						$\lvert p-90^\circ \rvert$
	126λ		487λ		973λ		
	E	W	E	W	E	W	
3C 230	0.80	--	--	--	--	0.55	00
3C 237	--	0.99	0.99	--	--	0.83	09
3C 243	--	--	0.67	--	--	--	08
3C 264	0.73	0.80	0.62	--	--	0.29	25
3C 270	--	0.78	0.23	0.28	0.04A		07
M 87	1.02	--	0.55	0.49	0.49	0.53	03
3C 278	--	0.98	0.70	0.71	0.28	0.27	15
3C 279	--	--	0.86	--	0.94	1.14	07
3C 283	1.00	--	1.00	--	--	0.99	28
3C 298	--	1.01	--	--	0.99A		08
MSH 14+010	--	--	0.91A		0.60A		04
3C 313	--	--	--	0.69	0.36	0.18	10
3C 317	--	--	--	0.98	0.94A		09
3C 318	--	--	--	1.02	0.92	0.92	26
3C 324	0.81	--	--	--	0.89	--	28
3C 327	1.02	--	--	0.50	0.56A		03
MSH 16+02	--	--	--	0.98	0.89A		02
3C 347	--	--	--	--	0.86	--	16
Herc A	0.98	--	--	--	0.21	0.17	06
3C 353	0.94	--	0.42A		0.34A		01
SN 1604	--	--	0.69	0.67	0.19	0.18	27
3C 365	--	--	0.96	--	1.00	0.46	16
Omega Neb.	0.77	--	0.16	0.07	0.09	0.02	20
3C 386	1.00	--	0.79	0.78	0.44	0.31	22
3C 397	0.66	--	--	0.38	--	0.05	08
3C 398	0.19	--	0.31	0.21	0.11	0.12	10
MSH 19-16	--	--	0.53	--	--	--	17
3C 403	--	--	0.68	--	0.25A		03
3C 413	--	--	0.77	--	--	--	09
3C 424	0.94	--	1.14	0.77	--	--	08
3C 433	--	--	--	--	0.96	--	33
3C 444	--	--	0.93	--	0.88	--	21
3C 445	--	--	0.73	--	0.51	--	03
3C 446	--	--	--	--	0.90	--	06
3C 456	--	--	0.75	--	0.75	--	11
3C 459	--	--	0.94	--	0.87	--	05

Note-- For the observations at an effective spacing of 126λ, the value of $\cos \theta_o$ was 0.646.

TABLE 7

VISIBILITY AMPLITUDES FOR OBSERVATIONS WITH $\cos \theta_o = 3/4$

Source	Effective Spacing						$\lvert p-90^\circ \rvert$
	292λ		584λ		1168λ		
	E	W	E	W	E	W	
3C 2	--	--	--	--	0.96 ± .08	----	00°
3C 17	--	--	1.05	--	---	----	02
3C 26	--	--	0.99	--	1.13 ± .19	----	03
3C 28	--	--	1.14	--	0.79 ± .07	----	25
3C 33	--	0.79	0.89	--	0.81 ± .05	----	11
3C 38	--	--	0.89	--	0.72 ± .04	----	14
3C 40	--	0.71	0.47	--	0.20 ± .08	----	01
3C 41	--	0.77	--	--	0.68 ± .04	----	35
3C 46	--	--	--	--	0.67 ± .22	----	43
3C 48	--	--	--	--	1.00 ± .05	----	35
3C 63	--	0.84	--	--	0.93 ± .10	----	02
MSH 02-110	--	0.88	--	--	0.84 ± .12	----	18
3C 71	--	0.97	--	--	0.91 ± .20	----	00
3C 75	--	0.71	--	--	0.24 ± .07	----	05
3C 78	--	0.88	--	--	0.67 ± .10	----	03
3C 79	--	0.97	--	--	0.50 ± .10	----	15
CTA 21	--	0.93	--	--	0.92 ± .12	----	15
CTA 26	--	0.91	--	--	---	----	02
3C 98	--	0.89	--	--	---	----	09
3C 109	--	0.96	--	--	---	----	10
3C 111	--	0.81	--	0.32	0.20 ± .04	0.32 ± .02	44
3C 123	standard source						30
3C 134	--	0.97	--	0.81	---	0.21 ± .03	44
3C 135	--	0.39	--	--	---	----	01
Crab Neb.	--	0.82	--	0.46	---	0.03 ± .00	21
Orion Neb.	--	0.46	--	0.17	---	0.03 ± .00	04
3C 154	--	0.92	--	0.83	---	0.85 ± .07	24
3C 161	--	1.00	--	0.99	---	0.98 ± .05	05
3C 175	--	0.89	--	0.88	---	0.76 ± .12	10
3C 180	--	0.93	--	0.81	---	0.84 ± .13	02
3C 191	--	0.89	--	0.92	---	1.18 ± .26	09
3C 198	--	0.71	--	0.33	---	0.27 ± .13	05
3C 208	--	1.06	--	0.75	---	0.74 ± .06	12
Hydra A	--	1.00	0.86	0.93	---	0.82 ± .05	10
3C 227	--	0.74	0.37	0.29	---	0.21 ± .04	06
3C 230	--	1.07	--	1.01	---	1.04 ± .12	00
3C 234	--	0.86	0.86	0.83	---	0.37 ± .06	29
3C 237	--	1.01	1.00	0.92	---	0.99 ± .10	06
3C 243	--	0.78	0.67A		---	0.67 ± .21	05
3C 264	0.61	0.65	0.52	0.52	0.30 ± .10	0.30 ± .03	18

TABLE 7 Continued

Source	Effective Spacing						$\lvert p-90^\circ \rvert$
	292λ		584λ		1168λ		
	E	W	E	W	E	W	
3C 265	0.87	1.07	0.76	--	---	0.68 ± .10	33
3C 270	0.27A		0.33A		0.04 ± .01A		05
3C 273	1.00A		0.99A		0.97 ± .04A		02
M 87	0.72	0.67	0.53	0.49	0.47 ± .02	0.49 ± .02	11
Coma A	0.88	1.06	--	0.97	---	1.04 ± .16	27
3C 278	0.79	0.85	0.59	0.58	0.18 ± .06	0.09 ± .03	11
3C 279	0.94A		0.97A		1.00 ± .05A		05
3C 283	1.01	1.01	--	--	---	----	21
3C 286	--	--	--	--	---	----	31
3C 287	0.96	0.92	0.95	0.95	0.86 ± .08	0.83 ± .06	25
3C 298	1.05A		0.97A		0.98 ± .07A		05
MSH 14+010	0.91A		--	--	---	0.54 ± .19	03
3C 310	0.84	0.96	0.72	--	0.16 ± .01	0.27 ± .04	26
3C 313	0.87A		0.67	--	0.26 ± .10	0.43 ± .06	07
3C 315	0.97	1.08	0.88	0.86	0.60 ± .09	0.67 ± .08	26
3C 317	0.99A		0.98A		0.93 ± .03A		06
3C 318	0.95	1.01	--	0.95	1.02 ± .14	0.91 ± .14	19
3C 324	0.93	0.99	0.79	--	0.85 ± .17	----	20
3C 327	0.77A		--	0.49	0.43 ± .03A		02
MSH 16+02	0.98	--	0.93	--	0.93 ± .05A		01
3C 338	0.87	--	--	--	0.63 ± .09	0.65 ± .14	47
3C 345	1.02	--	--	--	0.92 ± .08	0.59 ± .14	48
3C 347	0.62	--	0.71	0.44	0.71 ± .05	1.07 ± .21	11
Herc A	0.87	--	0.53A		0.39 ± .03A		04
3C 353	--	--	0.31A		0.39 ± .04A		01
SN 1604	0.93	--	0.60	0.58	<0.06	0.08 ± .02	20
Sgtr A	--	--	0.11	0.13	0.00	0.05 ± .00	29
3C 365	0.98	--	--	0.66	---	0.71 ± .15	12
Omega Neb.	0.42	--	0.15	0.03	0.05 ± .00	0.01 ± .00	14
CTA 80	0.94	--	0.88	--	0.72 ± .07	0.27 ± .05	34
3C 386	0.95	--	0.72	0.65	0.35 ± .05	0.27 ± .05	15
3C 397	0.39	--	0.31A		0.14 ± .02A		06
3C 398	0.63	--	0.26A		0.12 ± .01A		08
MSH 19-16	--	--	--	--	0.4 ± .26	----	13
3C 403	0.76	--	0.60	--	0.14 ± .05A		02
3C 409	--	--	--	--	1.02 ± .05A		22
CTB 87	0.66	--	0.27	--	0.21 ± .06	0.12 ± .04	42
3C 410	0.99	--	--	--	0.92 ± .09	----	30
3C 413	0.77	--	0.59	--	<0.67	----	06
3C 424	0.92	--	0.90	--	1.01 ± .17	1.12 ± .14	05
3C 433	0.95	--	--	--	0.91 ± .09	----	24
3C 436	0.71	--	--	--	0.68 ± .04	----	28
3C 438	0.95	--	--	--	0.86 ± .07	----	44
3C 444	0.97	--	0.94	--	0.90 ± .05	----	15
3C 445	0.89	--	0.82	--	0.35 ± .06	----	02

TABLE 7 Continued

Source	Effective Spacing						$\lvert p-90^\circ \rvert$
	292λ		584λ		1168λ		
	E	W	E	W	E	W	
3C 446	0.99	--	0.90	--	0.78 ± .09	----	04
CTA 102	0.94	--	--	--	---	----	10
3C 452	0.52	--	0.67	--	0.11 ± .05	----	47
3C 456	--	--	--	--	0.72 ± .14	----	08
3C 459	--	--	--	--	0.96 ± .09	----	03
MSH 23-112	--	--	--	--	1.14 ± .18	----	11
3C 465	--	--	0.28	--	0.23 ± .04	----	26

TABLE 8

VISIBILITY AMPLITUDES FOR OBSERVATIONS WITH $\cos \theta_o = 0.788$

Source	Effective Spacing		$\lvert p-90^\circ \rvert$
	1226λ		
	E	W	
3C 66	0.36	0.27	46°
3C 75	0.24	--	04
NGC 1275	0.63	0.70	42
3C 98	--	0.34	08
3C 111	0.19	0.36	36
3C 134	< 0.16	0.50	36

TABLE 9

VISIBILITY AMPLITUDES FOR OBSERVATIONS WITH $\cos \theta_o = 7/8$

Source	Effective Spacing						$\lvert p-90^\circ \rvert$
	169λ		681λ		1363λ		
	E	W	E	W	E	W	
3C 2	--	--	0.93	--	1.09	--	00
3C 20	--	0.94	0.87	--	0.83	--	47
3C 26	--	--	--	--	1.08	--	02
3C 28	--	--	--	--	0.86	--	17
3C 33	--	--	--	--	0.57	--	07
3C 38	--	--	--	--	0.76	--	10
3C 46	--	0.89	--	--	--	--	26
3C 66	--	0.82	--	--	0.08	--	32
3C 75	--	0.88	--	--	--	--	03
NGC 1275	--	0.93	--	--	0.66	0.66	30

TABLE 9 Continued

Source	Effective Spacing						|p-90°|
	169λ		681λ		1363λ		
	E	W	E	W	E	W	
Fornax A	--	0.13	--	--	--	--	26
3C 109	--	--	--	--	--	0.77	06
3C 111	--	0.91	--	--	--	0.33	26
3C 129	--	0.47	--	--	--	--	35
3C 134	--	0.94	--	--	--	--	27
3C 135	--	--	--	0.47	--	--	00
Crab Neb.	--	--	--	0.31	--	0.00	13
Orion Neb.	--	--	--	0.13	--	0.02	03
3C 161	--	--	--	0.01	--	--	03
3C 171	--	0.98	--	0.92	--	0.79	53
3C 175	--	--	--	--	--	0.58	06
3C 180	--	--	--	0.77	--	0.68	01
3C 198	--	--	--	0.34	--	0.16	03
3C 208	--	--	--	0.62	--	0.62	08
3C 216	--	0.98	--	--	--	--	35
Hydra A	--	--	--	0.88	--	0.81	06
3C 219	--	0.92	--	0.36	--	0.38	37
3C 227	--	--	0.31	0.19	--	0.20	04
3C 230	--	--	0.88	--	--	0.95	00
3C 237	--	--	1.01	1.02	--	1.06	04
3C 254	0.98	--	1.16	--	--	--	30
3C 264	--	--	0.52	0.49	0.39	0.22	12
3C 265	0.96	1.01	0.90	0.84	--	0.43	21
3C 270	--	--	0.32A		0.05A		03
3C 273	--	--	--	0.99	--	0.97	01
M 87	--	0.89	0.53	0.46	0.41	0.43	07
Coma A	1.05	--	--	--	--	0.97	18
3C 278	--	--	0.56	0.48	0.17	--	07
3C 279	--	--	--	--	0.89	--	03
3C 280	--	--	1.03A		1.01A		39
3C 283	--	--	--	0.96	--	--	13
3C 287	--	--	1.03	0.93	1.01	0.75	16
3C 298	1.06	--	--	--	1.01A		03
MSH 14+010	--	--	0.97A		0.62A		01
3C 310	0.95	0.98	0.60	0.73	0.11	0.27	17
3C 313	--	--	0.56	0.58	0.30	0.39	04
3C 315	--	--	0.84	0.69	0.54	0.59	17
3C 317	1.03	--	1.06	--	0.95	--	03
3C 324	--	--	0.95	0.85	0.89	--	13
3C 327	--	--	0.61	--	0.31	--	01
MSH 16+02	--	--	0.86	--	--	0.90	00
3C 338	1.02	--	--	0.85	0.52	0.45	28
3C 345	1.05	--	--	0.88	1.10	0.89	29
3C 347	--	--	0.84	0.69	0.68	0.49	07
Herc A	--	--	0.40A		0.56A		02

TABLE 9 Continued

Source	Effective Spacing						$\lvert p-90^\circ \rvert$
	169λ		681λ		1363λ		
	E	W	E	W	E	W	
3C 353	--	--	0.25	--	--	--	00
SN 1604	--	--	--	0.50	0.10	0.10	13
Sgtr A	--	--	--	0.11	0.03	0.02	18
Omega Neb.	--	--	--	0.03	--	0.02	09
CTA 80	1.02	--	0.77	0.35	0.39	0.21	22
3C 386	1.02	--	0.66	0.64	--	0.22	10
3C 388	0.85	--	0.78	0.64	0.80	0.65	36
3C 397	--	--	0.21A		--	--	03
3C 398	--	--	0.04A		0.10A		05
MSH 19-16	--	--	< 0.6	--	--	--	08
3C 402	--	--	0.41	--	0.21	--	44
Cygnus A	--	--	--	--	0.31	0.24	29
CTB 87	0.80	--	0.42	--	0.16	--	25
3C 410	--	--	1.01	--	0.95	--	19
3C 413	--	--	0.61	--	--	--	04
3C 424	--	--	0.95	--	0.88	--	03
3C 433	--	--	--	--	1.00	--	16
3C 436	--	--	0.75	--	0.62	0.68	18
3C 438	--	--	0.94	--	1.00	--	26
3C 445	--	--	0.56	--	--	0.08	01
3C 446	--	--	0.76	--	--	--	02
3C 452	--	--	0.30	--	0.26	--	28
3C 465	--	--	0.28	--	0.11	--	17

Note-- For the observations at an effective spacing of 169λ, the value of $\cos \theta_o$ was 0.867.

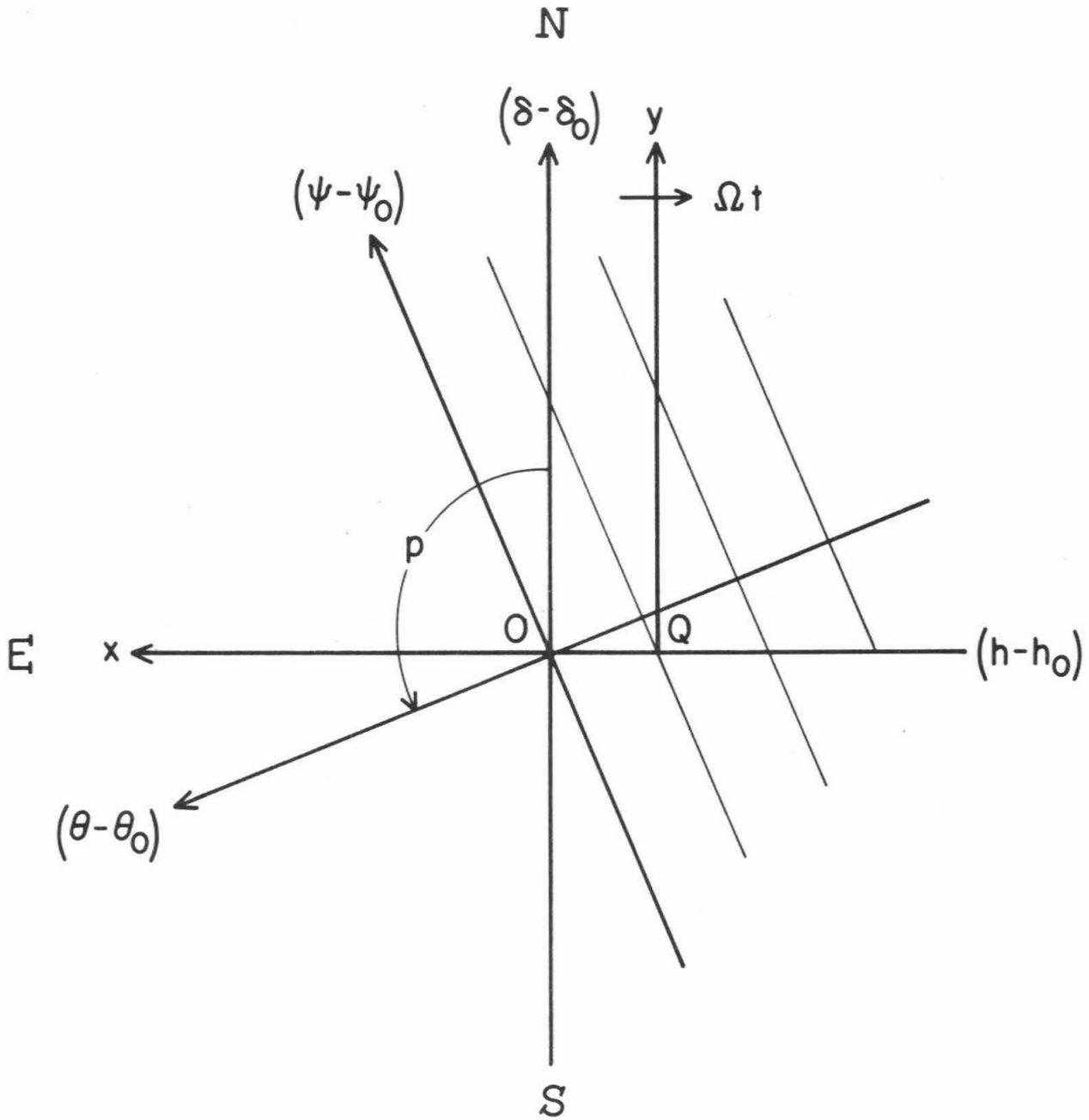

Fig. 1.--The h,δ, θ,ψ, and x,y coordinate systems in the neighborhood of the point O at h_0,δ_0. The centroid of the source is at point Q. The fine lines of constant θ represent the crests of successive fringes.

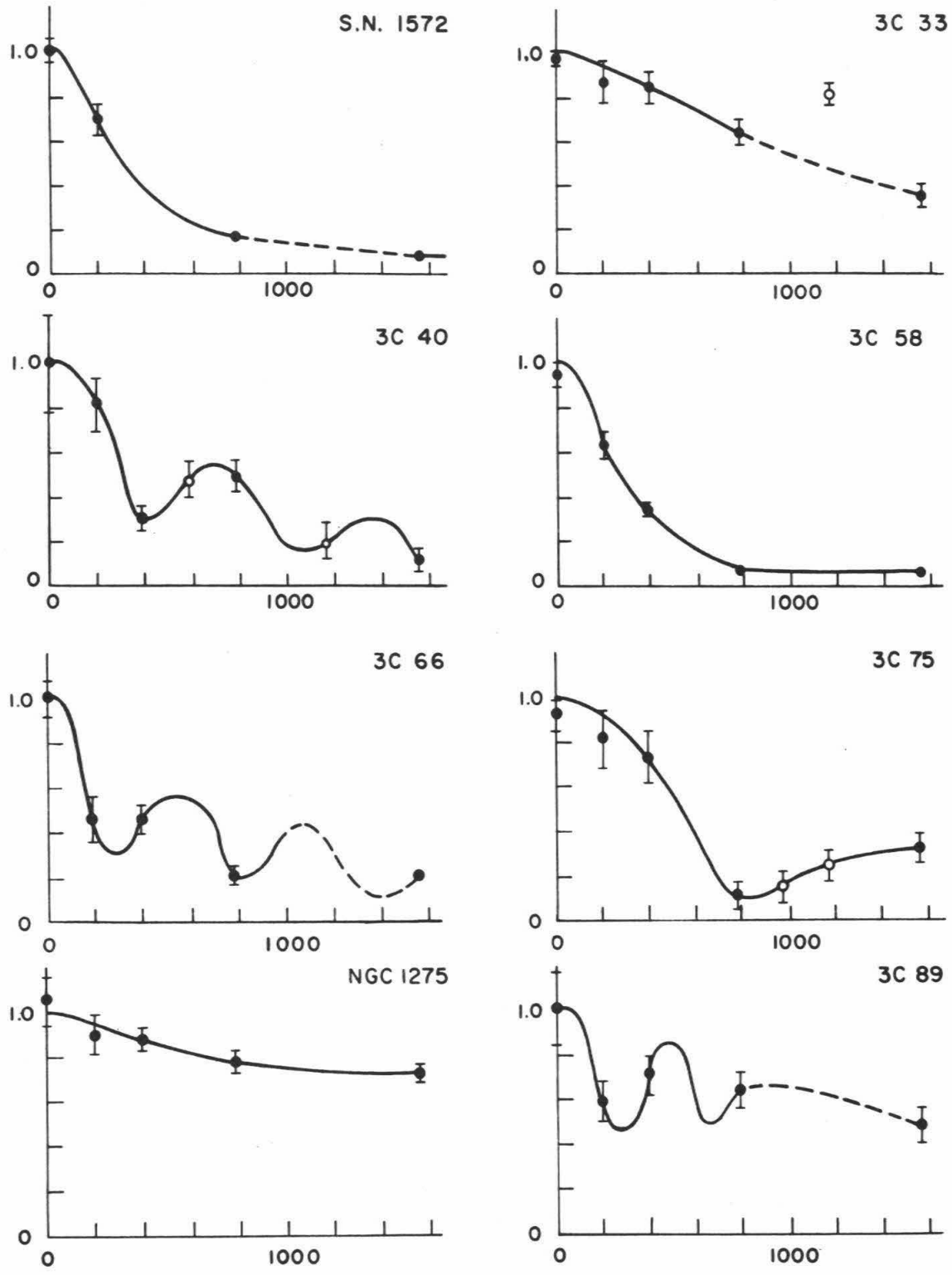

Fig. 2.--Visibility amplitudes for S.N. 1572, 3C 33, 3C 40, 3C 58, 3C 66, 3C 75, NGC 1275, and 3C 89. Abscissae are antenna spacings, in wavelengths.

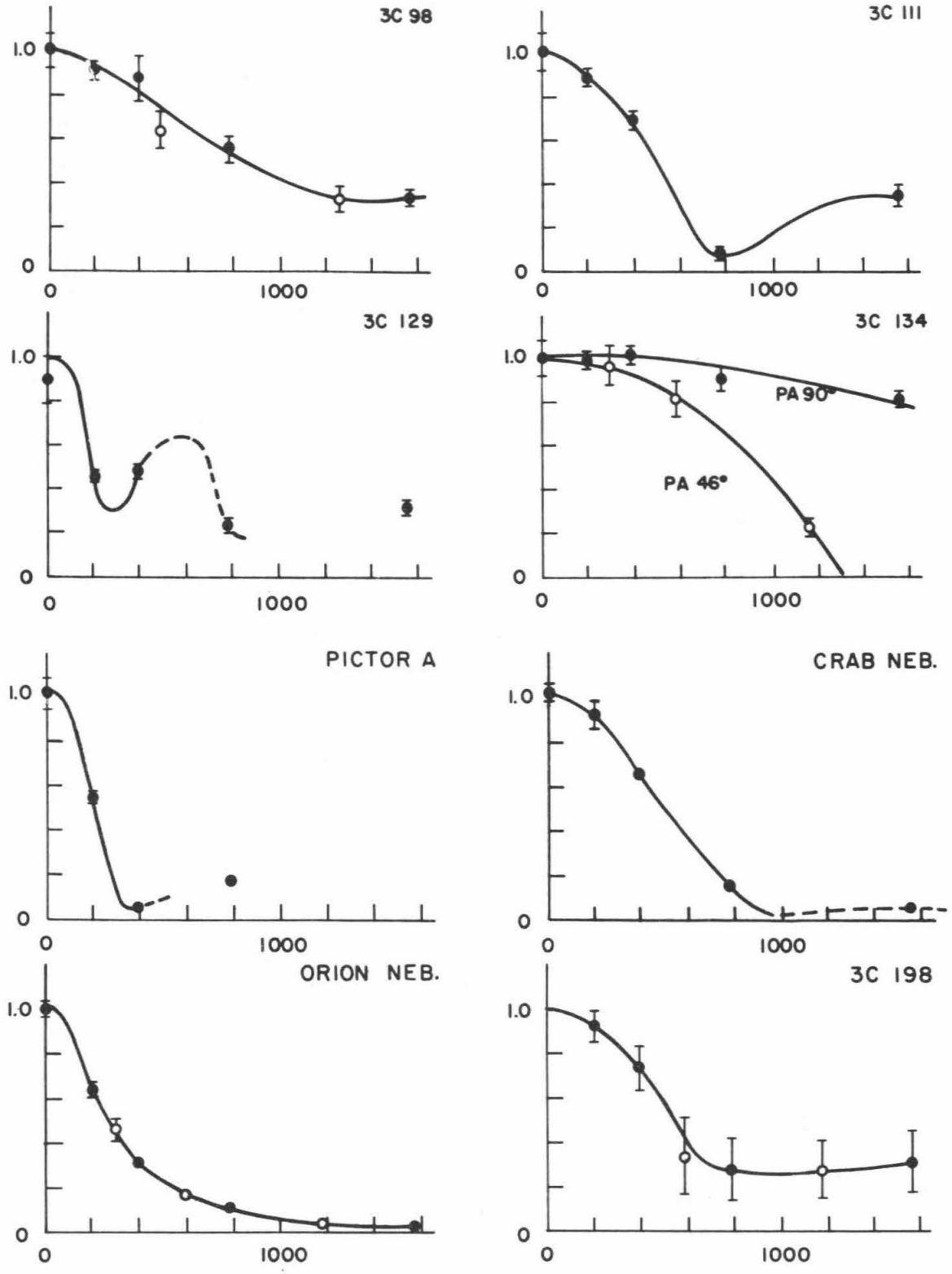

Fig. 3.--Visibility amplitudes for 3C 98, 3C 111, 3C 129, 3C 134, Pictor A, Crab Nebula, Orion Nebula and 3C 198. Abscissae are antenna spacings, in wavelengths.

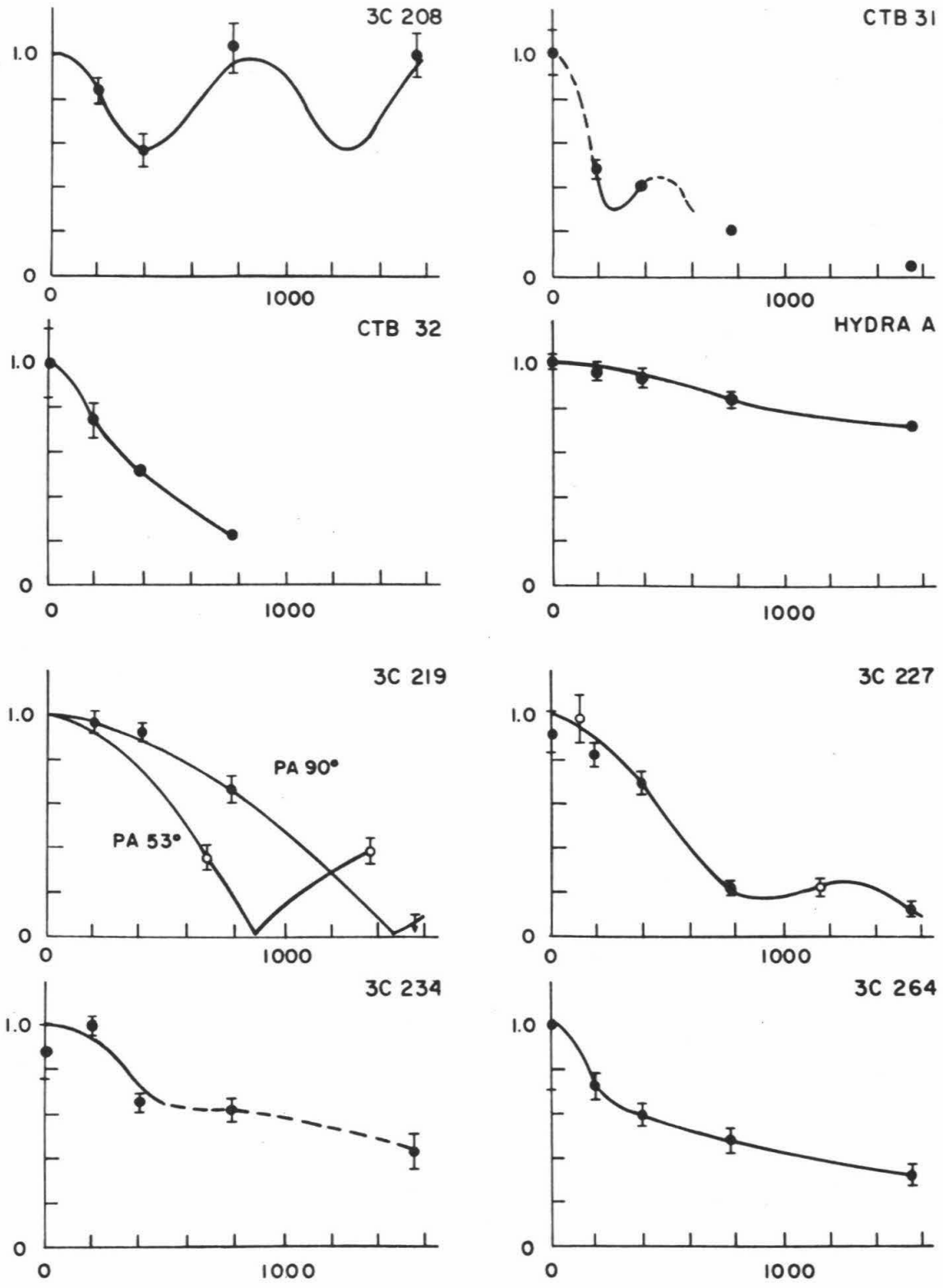

Fig. 4.--Visibility amplitudes for 3C 208, CTB 31, CTB 32, Hydra A, 3C 219, 3C 227, 3C 234, and 3C 264. Abscissae are antenna spacings, in wavelengths.

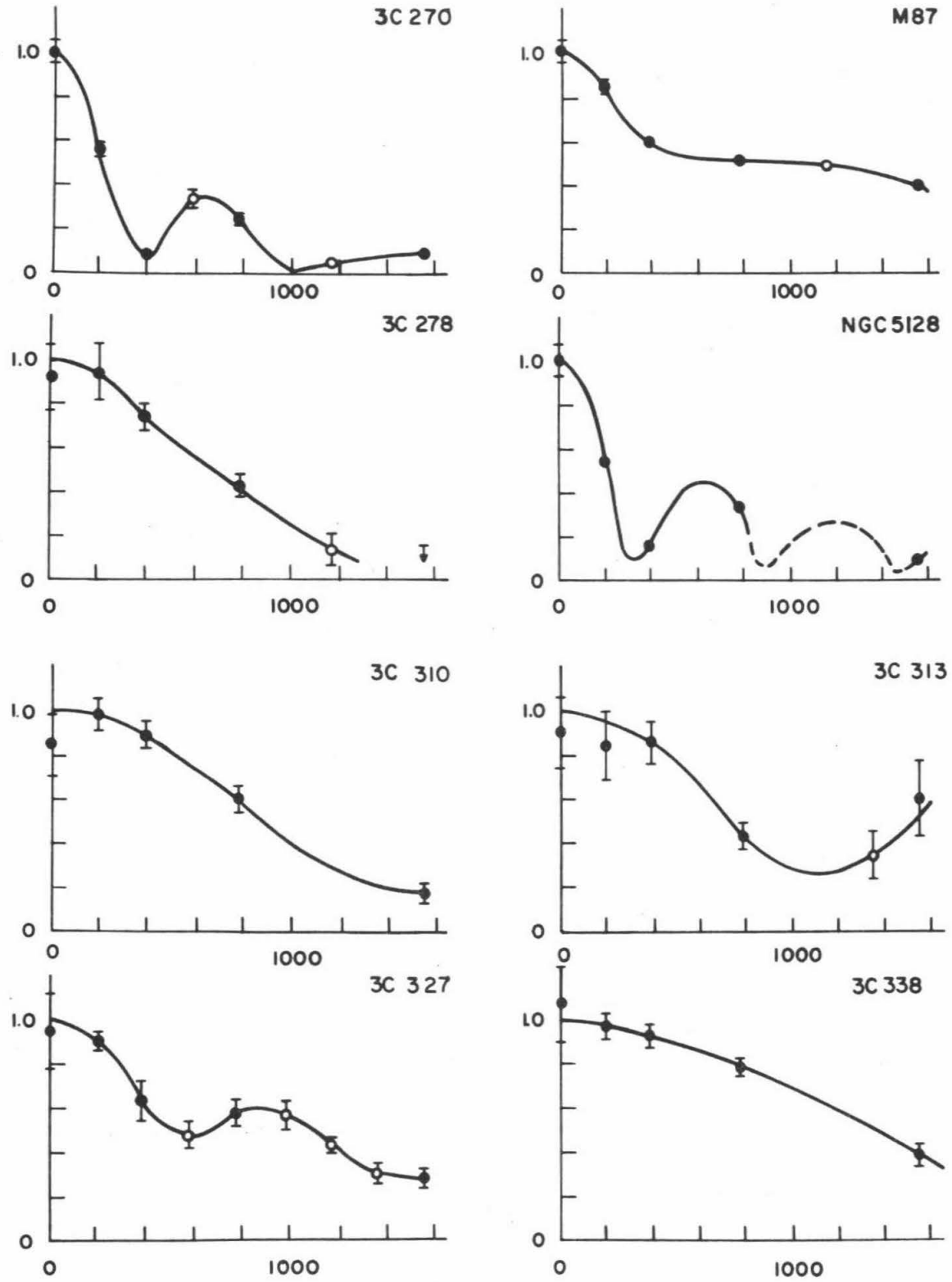

Fig. 5.--Visibility amplitudes for 3C 270, M87, 3C 278, NGC 5128, 3C 310, 3C 313, 3C 327, and 3C 338. Abscissae are antenna spacings, in wavelengths.

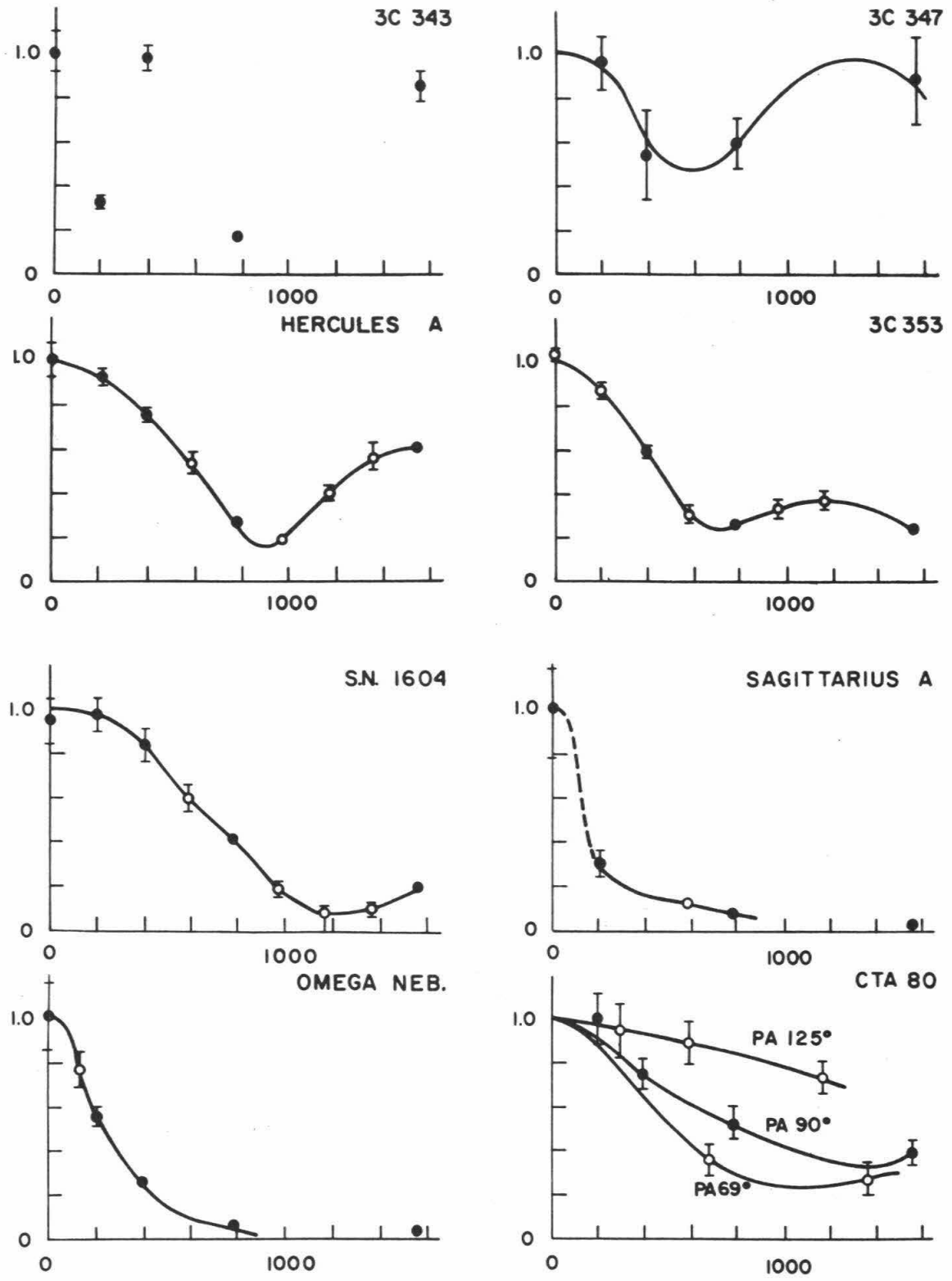

Fig. 6.--Visibility amplitudes for 3C 343, 3C 347, Hercules A, 3C 353, S.N. 1604, Sagittarius A, Omega Nebula and CTA 80. Abscissae are antenna spacings, in wavelengths.

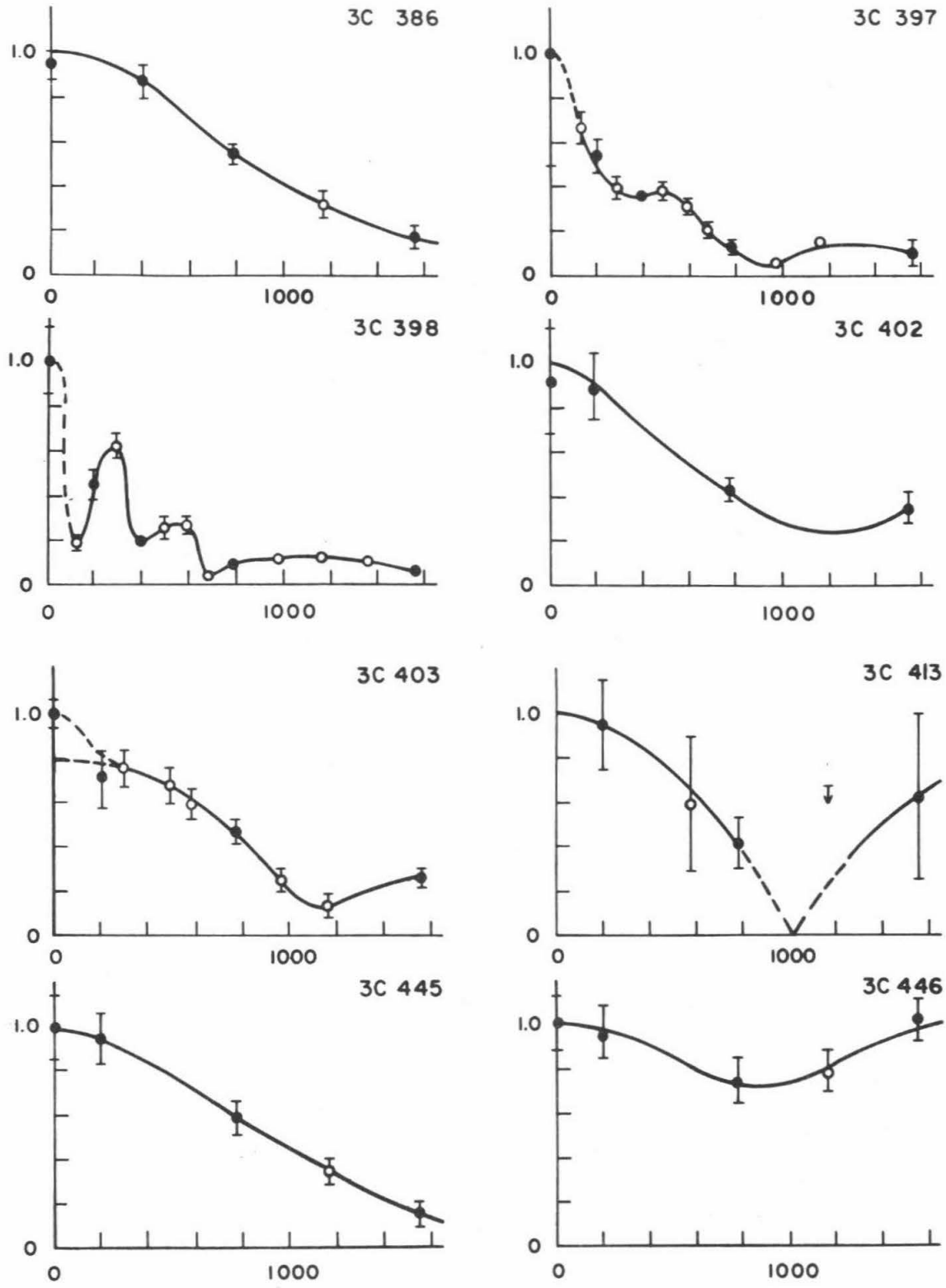

Fig.7.--Visibility amplitudes for 3C 386, 3C 397, 3C 398, 3C 402, 3C 403, 3C 413, 3C 445, and 3C 446. Abscissae are antenna spacings, in wavelengths.

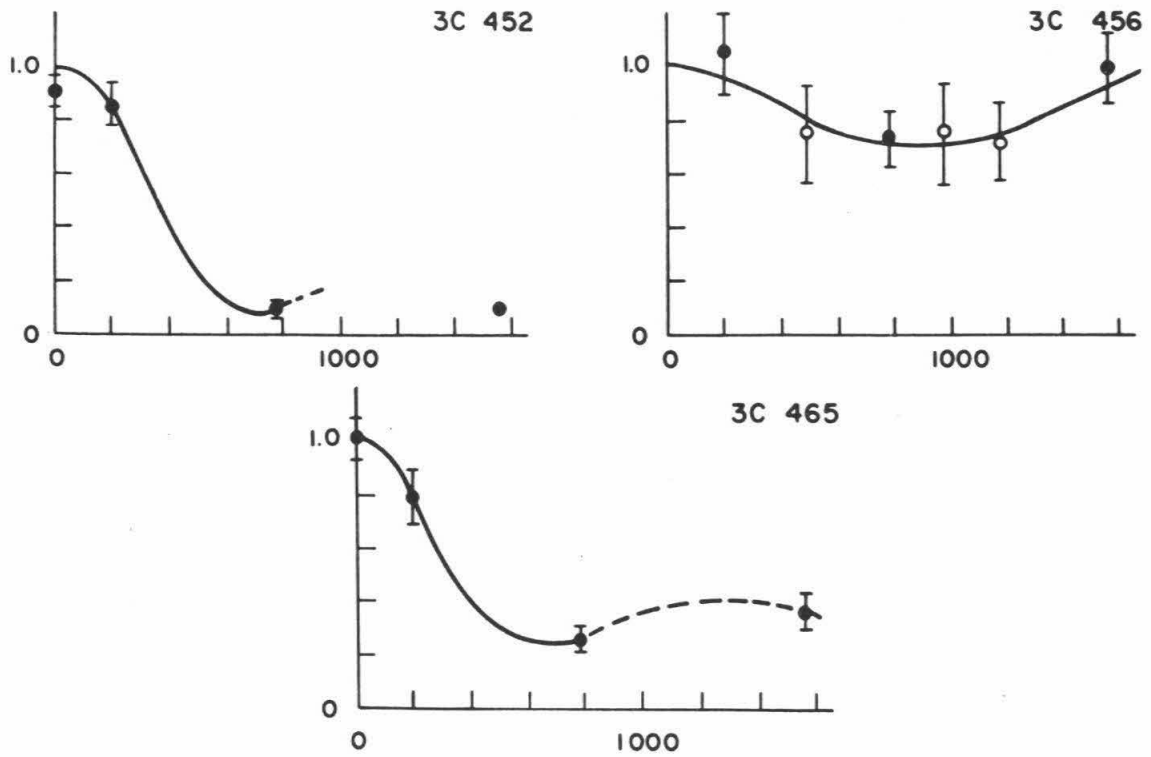

Fig. 8.--Visibility amplitudes for 3C 452, 3C 456, and 3C 465. Abscissae are antenna spacings, in wavelengths.

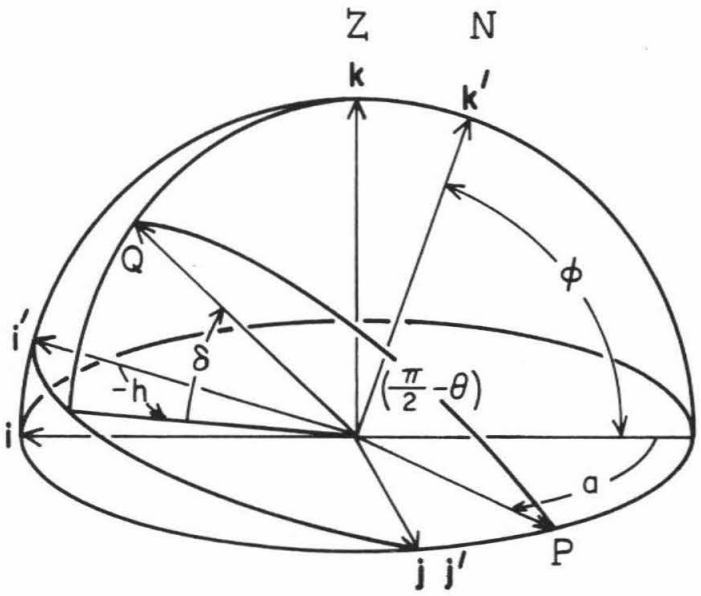

Fig. 9.--The derivation of $\sin\theta$.